



Chemical Composition, Optical Properties and Sources of PM_{2.5} From a Highly Urbanized Region in Northeastern Mexico

Karim Acuña Askar¹, Lucy T. González^{2*}, Alberto Mendoza², Oxana V. Kharissova³, Andrea Rodríguez-Garza², Eleazar M. Lara⁴, Alfredo Campos⁵, D. López-Serna⁴, Lilia M. Bautista-Carrillo⁶, J. M. Alfaro-Barbosa⁴ and F. E. Longoria-Rodríguez⁶

¹Universidad Autónoma de Nuevo León, Facultad de Medicina, Laboratorio de Biorremediación Ambiental, Monterrey, México, ²Tecnológico de Monterrey, Escuela de Ingeniería y Ciencias, Monterrey, México, ³Universidad Autónoma de Nuevo León, Facultad de Fisicomatemáticas, Centro de Innovación, Investigación y Desarrollo en Ingeniería y Tecnología, Monterrey, México, ⁴Universidad Autónoma de Nuevo León, Facultad de Ciencias Químicas, Laboratorio de Química Analítica Ambiental, Monterrey, México, ⁵Centro de Investigación en Materiales Avanzados S.C. (CIMAV), Chihuahua, México, ⁶Centro de Investigación en Materiales Avanzados S.C. (CIMAV), Unidad Monterrey, Apodaca, México

OPEN ACCESS

Edited by:

Michael MacKinnon,
University of California, Irvine,
United States

Reviewed by:

Bighnaraj Sarangi,
University of Puerto Rico, Puerto Rico
Beatrice Moroni,
University of Perugia, Italy

*Correspondence:

Lucy T. González
lucy.gonzalez@tec.mx

Specialty section:

This article was submitted to
Toxicology, Pollution and the
Environment,
a section of the journal
Frontiers in Environmental Science

Received: 26 April 2022

Accepted: 08 June 2022

Published: 04 July 2022

Citation:

Acuña Askar K, González LT, Mendoza A, Kharissova OV, Rodríguez-Garza A, Lara EM, Campos A, López-Serna D, Bautista-Carrillo LM, Alfaro-Barbosa JM and Longoria-Rodríguez FE (2022) Chemical Composition, Optical Properties and Sources of PM_{2.5} From a Highly Urbanized Region in Northeastern Mexico. *Front. Environ. Sci.* 10:929449. doi: 10.3389/fenvs.2022.929449

Here, we report the chemical composition and optical properties of the fine particles (PM_{2.5}) and water-soluble organic carbon (WSOC) of these particles. Additionally, the potential sources of WSOC emission were determined through the study on fluorescence excitation–emission matrix spectra and parallel factor analysis (EEM-PARAFAC). Samples were collected in an urban site of the Monterrey Metropolitan Area in Mexico during summer and winter and characterized using attenuated total reflectance-Fourier-transform infrared spectroscopy (ATR-FTIR), ultraviolet-visible-near infrared-diffuse reflectance spectroscopy (UV-Vis-NIR-DRS), fluorescence spectroscopy, X-ray photoelectron spectroscopy (XPS), and X-ray diffraction (XRD) techniques. The ATR-FTIR analyses allowed the identification of inorganic ions (e.g., CO₃²⁻, SO₄²⁻, and NO₃⁻), organic functional groups [e.g., carbonyls (C=O), organic hydroxyl (C-OH), carboxylic acid (COOH)], and aromatic and unsaturated aliphatic hydrocarbons. The results obtained by XRD and XPS revealed the presence of organic and inorganic chemical species in PM_{2.5}. The diffuse reflectance spectra of PM_{2.5} provided the absorption bands in the UV region for CaSO₄, CaCO₃, and aluminosilicates. The absorption coefficient at 365 nm (Abs₃₆₅) and Ångström absorption exponent (AAE) values obtained for the aqueous extracts suggest that many of the water-soluble organic compounds corresponded to brown carbon (BrC) chromophores. The mass absorption efficiency values at 365 nm (MAE₃₆₅) were higher in the winter than summer samples, suggesting the presence of more BrC compounds in the winter samples. The fluorescence indices combined with

Abbreviations: ATR, Attenuated total reflection; DOM, Dissolved organic matter; DRS, Diffuse reflectance spectroscopy; EC, Elemental carbon; FI, Fluorescence index; HULIS, Humic-like substances; MAE, Mass absorption efficiency; MMA, Monterrey metropolitan area; MS, Mass spectrometry; NIST, National institute of standards and technology; OC, Organic carbon; PM, Particulate matter; SIMA, Sistema integral de monitoreo ambiental; TOC, Total organic carbon; VOC, Volatile organic compounds; WSOC, Water-soluble organic carbon; XPS, X-ray photoelectron spectroscopy; XRD, X-ray diffraction.

EEM-PARAFAC analysis showed that the WSOC fraction was mainly composed of humic-like substances (HULIS) which are both of terrestrial and microbial origin.

Keywords: PM_{2.5}, mass absorption efficiency (MAE), water-soluble organic carbon (WSOC), parallel factor analysis (PARAFAC), Ångström absorption exponent

1 INTRODUCTION

The extensive atmospheric pollution occurring in large cities as a result of fast-growing urban and industrial development has caused an increase in the number of people to be continuously exposed to low-quality ambient air. Particulate matter (PM) is a common atmospheric pollutant, which has been widely studied because of its adverse effects on both the public health and global climate. Particularly, fine PM (PM_{2.5}) has been considered more dangerous because it is able to penetrate the deep parts of the human lung. Indeed, numerous studies have associated the components of PM_{2.5} to many respiratory (e.g., lung cancer) and cardiovascular diseases. These components have also been found to cause genetic mutations in animals (Lippmann et al., 2006; Happonen et al., 2010). In addition to the adverse effects on animal and human health, PM_{2.5} influences both local and global climates. Several PM_{2.5} components have been shown to cause the dispersion and absorption of light (including infrared light). These effects on light disturb the radiation balance of the atmosphere, which may then cause unexpected variations in the atmospheric heating-cooling cycles (Jacobson, 2004; Huo et al., 2016; Chen et al., 2019). Our present knowledge related to the influence of PM_{2.5} on radiative forcing (change in energy flux in the atmosphere) and climate change is still limited. Moreover, there are difficulties associated with the current atmospheric models, which are used to measure the magnitude of both capture and release of radiation by PM_{2.5}. For example, different types of aerosols may exert a large range of contrasting effects on the net cooling or heating of an atmosphere. This is caused by the high variability of the PM_{2.5} properties in the atmospheric aerosols as a function of the region.

PM_{2.5} is composed of a wide variety of chemical substances of both organic and inorganic origin, being carbonaceous material the component that has attracted the most attention because they contribute between 10% and 70% of the total mass of PM_{2.5}, with concentrations found in selected areas ranging from a few pg/m³ to hundreds of ng/m³ (Tsapakis et al., 2002; Hecobian et al., 2010; Khare et al., 2011). Black carbon (BC) is the main light-absorbing carbonaceous material in the range from visible to near infrared light. However, the fraction of organic carbon (OC) that is often called “Brown Carbon (BrC)” has also been found to significantly absorb ultraviolet (UV) and shorter wavelength visible (Vis) light (Jacobson, 2001; Bond et al., 2004). The contribution of BrC to climate change is not limited to its impact to the atmosphere due to its ability and capacity to absorb solar radiation. Recent studies have shown that BrC has accelerated the melting of snow and decreased the Earth’s albedo (Andreae and Ramanathan, 2013; Qian et al., 2015; Yan et al., 2018; Leskinen et al., 2020). Some researchers have classified OC based on its water solubility, i.e., the water-soluble organic carbon (WSOC) and water-insoluble organic carbon (Kondo et al., 2007; Miyazaki et al., 2009). The analyses of

the optical properties of WSOC have allowed the identification of its probable emission sources, and thus provided helpful strategies to control emission. In the literature it has been reported that WSOC originates from either primary sources (biomass burning, fossil fuel combustion) or atmospheric secondary processes, including gas-to-particle conversion and gas deposition onto the surface of a PM (Graber and Rudich, 2006; Sullivan and Weber, 2006; Duarte et al., 2007).

The study of the optical properties of atmospheric particles requires a variety of analytical techniques, including Fourier-transform infrared (FTIR) and UV-Vis spectroscopy, fluorescence, mass spectrometry (MS), and chromatography. Hecobian et al. (2010) characterized the optical properties of the water-soluble fraction of PM_{2.5} samples using various analytical techniques. Their samples were collected in the southeastern United States throughout different seasons of a year. They found that the WSOC absorption was higher in the samples obtained during the cold months. The WSOC content was closely related to the presence of levoglucosan in the sample, suggesting that biomass burning was the main source of the emission. Moreover, Chen et al. (2016a) studied the relationship between the optical properties and chemical composition of total suspended PM in samples using FTIR, UV-Vis, fluorescence spectroscopy, electrospray ionization mass spectrometry (ESI-MS) and high-resolution accurate mass spectrometry (HR-AMS). They found that the mass absorption efficiency (MAE) was higher for the less polar organic compounds in the sample. In addition, the nitrogen and oxygen containing organic compounds contributed significantly to the total absorption of light and fluorescence of PM.

The Monterrey Metropolitan Area (MMA) has been considered the most polluted city in Mexico and one of the most polluted cities in Latin America (Clean Air Institute, 2012; INECC, 2014). The elevated emissions in the MMA originate mainly from the high industrial activity and vehicle traffic. However, studies on the chemical composition of atmospheric PM and optical properties of PM_{2.5} in the MMA have been limited (Mancilla et al., 2015; Mancilla et al., 2016; Mancilla et al., 2019; González et al., 2016; González et al., 2017; González et al., 2018; López-Ayala et al., 2019; Longoria-Rodríguez et al., 2020; Longoria-Rodríguez et al., 2021). There is also limited information on the absorption response and light emission of PM_{2.5} in Mexico after exposure to variable wavelengths of radiation (Liñán-Abanto et al., 2019; Carmona et al., 2021). Furthermore, studies on the chemical and optical characteristics of WSOC in PM_{2.5} in Mexico and other Latin American countries have not been done. Therefore, this research focuses on three main objectives; 1) determine the chemical composition and optical properties of PM_{2.5} collected in the MMA during winter and summer, 2) determine the effect of seasonal variation on the chemical composition and optical properties of the PM_{2.5}, and 3) establish possible sources of

TABLE 1 | Statistical summary of the meteorological variables recorded during both study periods. SD: Standard deviation.

Meteorological parameter	Winter		Summer	
	Average	SD	Average	SD
Pressure (mmHg)	719.7	7.2	708.5	4.1
Relative humidity (%)	59.5	20.6	56.9	16.3
Solar radiation (W/m ²)	145.4	222.8	238.9	273.1
Room temperature (°C)	21.1	6.3	35.9	2.9
Wind speed (km/h)	8.6	4.7	14.4	0.6
Wind Direction (degree)	15.0	67.0	136.9	83.2

WSOC emissions in MMA by applying the parallel factor analysis (PARAFAC) model. The analytical techniques including attenuated total reflection (ATR)-FTIR, UV/VIS-diffuse reflectance spectroscopy (DRS), fluorescence, x-ray diffraction (XRD), and x-ray photoelectron spectroscopy (XPS) were used to determine the optical properties and chemical composition of the PM_{2.5} samples.

2 METHODOLOGY

2.1 Sampling of PM_{2.5}

The sampling site was in the northwestern region of the MMA in Nuevo Leon, Mexico. PM_{2.5} sampling was performed at the routine monitoring station of the Integral Environmental Monitoring System [Sistema Integral de Monitoreo Ambiental (SIMA), the initials in Spanish] located in the San Bernabé suburb (25° 45' 24.86"N, 100° 21' 56.95"W, 551 m. a.s.l.) near the Talleres subway station. This station is surrounded by a highly populated urban area and located alongside the westward winds, which is coming from the highest density industrial area of MMA. In addition, it lies near a natural reserve Mount del Topo Chico. PM_{2.5} samples were collected during July to August 2019 and January to February 2020 following the Method IO-2.1 USEPA method (U.S. EPA. Environmental Protection Agency Methods, 1999), where sampling temperature, relative humidity, and atmospheric pressure conditions were recorded (Table 1). The samples were collected every 6 days, collecting a total of 8 samples in each period.

A high-volume sampler HiVol 3000 from Ecotech, which was previously calibrated according to Method IO-2.1 USEPA (U.S. EPA. Environmental Protection Agency Methods, 1999) was placed at the SIMA station. PM_{2.5} samples were collected for 24 h on fiberglass filters (EPM 2000 of 8" × 10"), with a mean airflow of 67 m³/h. For the sampling, glass fiber filters were chosen instead of quartz filters since glass is a material that does not interfere with the analyzes by the XRD technique. The mass of a loaded filter was determined using an analytical balance XS205 dual range from Mettler Toledo under a controlled relative humidity. The filter was stored at -15°C when not in use.

2.2 Optical Analysis of PM_{2.5} Samples

2.2.1 ATR-FTIR Analysis

Chemical functional groups present in the PM_{2.5} were identified by ATR-FTIR using a Nicolet omnic iS50 FTIR spectrophotometer from Thermo Fisher Scientific.

Measurements were made in ATR mode using an ATR Smart Orbit accessory supplied with a diamond crystal. All spectra were recorded at a resolution of 4 cm⁻¹ over the spectral range from 4,000 to 400 cm⁻¹. The absorption path length and total data points were 1 cm and 7,468, respectively. A scan was performed with the sample placed upside down on the ATR crystal (diameter = 3 mm). The background correction was performed by subtracting the absorption spectrum of the filter without sample from that obtained for the loaded filters. Samples did not require any pre-treatment and were analyzed directly on the fiberglass filters. The resulting set of data with baseline correction was analyzed using the SpectraGryph 1.2 Spectroscopy software (Menges, 2020).

2.2.2 UV-Vis Absorption Profiles of PM_{2.5}

PM_{2.5} samples were characterized using the UV-Vis-NIR-DRS technique. The UV-Vis-NIR-DRS spectra were obtained with an Agilent Model Cary 5000 spectrometer equipped with an external integration sphere DRA 2500 from Agilent Technologies. The analysis was carried out directly on a filter at an area of 0.3 cm². The absorption path length was 1 nm. The filter blank was measured before the analysis. Prior to each measurement, baseline corrections were performed at both 0% and 100% transmittance. Samples were analyzed over the range from 200 to 2,500 nm with a resolution of 2 nm, which resulted in 2,301 data points.

2.2.2.1 Analysis of Water-Soluble Organic Carbon Fraction by UV-Vis

For WSOC fraction extraction, 10% of the total area of a filter (and filter blanks) was extracted with 30 ml of purified water in an ultrasonic bath for 15 min. The purified water was obtained from a Milli-Q system from Merck Millipore (Burlington, MA, United States). The extraction procedure was repeated twice. The extract was filtered through a 25-mm outer diameter polytetrafluoroethylene (PTFE) syringe filter of 0.22 μm pore size from Tisch Scientific. Approximately 3 ml of the filtered extract (WSOC solution) was placed in a 1-cm quartz cuvette and scanned from 200 to 800 nm in 1 nm increments using the Agilent Model Cary 5000. Purified water was used as both blank reference and baseline source of data.

The light absorption coefficient (Abs_λ, Mm⁻¹) was determined by Eq. 1 (Teich et al., 2017):

$$\text{Abs}_\lambda = (A_\lambda - A_{700}) \frac{Vl}{Va \times L} \times \ln(10) \quad (1)$$

where A_λ and A₇₀₀ corresponded to the absorption of the extracts at the wavelengths of λ and 700 nm, respectively. Vl was the volume of the solvent that the sample extract removed from the filter, Va was the air volume, and L was the absorption path length (i.e., 1 cm). The light absorption coefficient at 365 nm (Abs₃₆₅) was used as the indicator of BrC (Wu et al., 2019; Mo et al., 2021). Furthermore, the mass absorption efficiency at 365 nm (MAE₃₆₅, m²g⁻¹C) was measured. MAE is a parameter that described the

light absorbing ability of WSOC. This parameter was determined by Eq. 2 (Chen et al., 2018):

$$\text{MAE}_{365} = \frac{\text{Abs}_{365}}{C_{\text{WSOC}}} \quad (2)$$

where C_{WSOC} represented the WSOC concentration in $\mu\text{gC}/\text{m}^3$. The WSOC concentration was determined using a total organic carbon (TOC) analyzer model TOC-VCSH from Shimadzu (Kyoto, Japan). During the analysis, the supply gas pressure, carrier gas flow, and furnace temperature were set at 200–250 kPa, 150 ml min^{-1} , and 680°C, respectively. The sample was acidified and injected into the analyzer oven. In the oven, the carbon was catalytically oxidized to CO_2 at 680°C and the produced CO_2 was detected by the sensitive Nondispersive Infrared (NDIR) detector ($2,500 \text{ cm}^{-1}$). Moreover, the wavelength dependence and light absorption of a water extract was investigated by the Ångström absorption exponent (AAE) in the wavelength range from 300 to 600 nm by Eq. 3 (Moosmüller et al., 2011).

$$\text{AAE} = \frac{\ln(\text{Abs}_{\lambda 2}) - \ln(\text{Abs}_{\lambda 1})}{\ln(\lambda 2) - \ln(\lambda 1)} \quad (3)$$

2.2.3 Analysis of PM_{2.5} by Fluorescence Spectroscopy

The fluorescence of PM_{2.5} particles was measured by placing a small portion of a filter (0.5 cm^2) in the sample holder of a spectrofluorometer Model FluoroMax-4 from Horiba, which was supplied with a vertically assembled xenon-arc lamp set at 150 W without ozone. The excitation wavelength was 355 nm and the emission wavelength ranged from 400 to 700 nm, with slit set to 5 nm for both the excitation and emission monochromators and using a 0.1 s integration time. The detected signals were provided by a photon-counting detector R928P PMT (185–850 nm). A photodiode array was used to monitor the lamp output.

The excitation–emission matrices (EEMs) of the WSOC fractions were measured in the range from 200 to 600 nm for excitation and 220–600 nm for emission. The band passes for excitation and emission were 20 and 1 nm, respectively. Three fluorescence indices were evaluated including the fluorescence index (FI), biological index (BIX), and humification index (HIX). These indexes have been implemented in studies involving DOM in both soil and aquatic systems and aerosol due to the similarities in the optical aspects of WSOC and aquatic DOM. Indeed, these indexes have been shown to provide some information on the nature of the organic compounds present in the water-soluble fraction of aerosols (McKnight et al., 2001; Huguet et al., 2009; Birdwell and Engel, 2010). The fluorescence parameters FI, BIX, and HIX were evaluated by Eqs 4–6, respectively.

$$\text{FI} = \frac{F(\text{Ex} = 370 \text{ nm}, \text{Em} = 450 \text{ nm})}{F(\text{Ex} = 370 \text{ nm}, \text{Em} = 500 \text{ nm})} \quad (4)$$

$$\text{BIX} = \frac{F(\text{Ex} = 310 \text{ nm}, \text{Em} = 380 \text{ nm})}{F(\text{Ex} = 310 \text{ nm}, \text{Em} = 430 \text{ nm})} \quad (5)$$

$$\text{HIX} = \frac{F(\text{Ex} = 255 \text{ nm}, \text{Em} = 434 - 480 \text{ nm})}{F(\text{Ex} = 255 \text{ nm}, \text{Em} = 300 - 345 \text{ nm})} \quad (6)$$

where F represents the fluorescence intensity and Ex and Em the excitation and emission wavelengths, respectively. In the literature, $\text{FI} < 1.4$ has been attributed to the fluorophores of terrestrial fulvic acid with greater aromaticity, while values higher than 1.9 correspond to fluorophores from microbial emissions of lower aromaticity (McKnight et al., 2001; Wu et al., 2021). The BIX value is used to assess the contributions from microbial activities, $\text{BIX} > 1$ indicates the predominant biological or microbial formation, while $\text{BIX} < 0.6$ corresponds to an autochthonous component with smaller contribution from biological materials (Huguet et al., 2009; Wen et al., 2021; Wu et al., 2021). HIX value represents the degree of humification of organic matter, higher values ($\text{HIX} > 10$) are attributed to more humic or aromatic organic matter associated with terrestrial sources, while lower values ($\text{HIX} < 5$) are associated with organic matter freshly formed (Yang et al., 2020). Finally, to support the information provided by the fluorescence indices, the PARAFAC model was applied. Recently, some researchers have reported the importance of using fluorescence indices and the PARAFAC model to establish possible sources of emission of carbonaceous material in the aqueous fraction. PARAFAC is a statistical model approach that extracts independent fluorophores from EEMs under ideal conditions (Bro, 1997). The determination of the component number and the treatment of the spectroscopic data, which included the biases correction, scattering remove and normalization, was carried out by applying the staRdom software [“spectroscopic analysis of dissolved organic matter (DOM) in R”]. (Pucher et al., 2019).

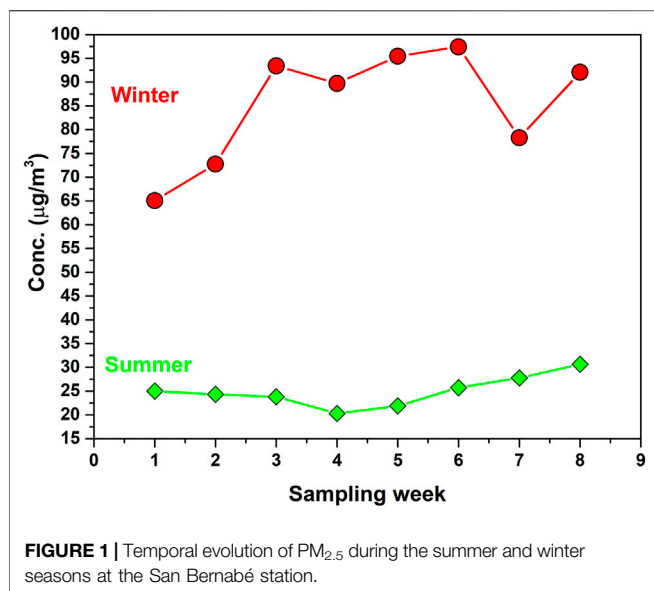
2.3 Mineralogical and Chemical Analysis

2.3.1 Chemical Surface Analysis of PM_{2.5} Using X-Ray Photoelectron Spectroscopy

The XPS technique was used to determine the surface chemical composition of PM_{2.5}. For this purpose, a Thermo Scientific Escalab 250Xi spectrometer with both a six-channel (channeltron) detector and a monochromatic X-ray Al K α source (1486.68 eV) was used. A selected 1 cm^2 piece from the center of each filter was cut and placed on the sample holder using carbon tape. Measurements were read while keeping ultrahigh vacuum conditions (10^{-10} torr). Survey spectra for all the samples were collected over the 1100 eV range at a resolution of 1 eV per step, 100 ms, and 150 eV of pass energy. For the chemical species of interest, high-resolution spectra were collected at a resolution of 0.1 eV per step and 20 eV of pass energy. For data treatment, Avantage software (Thermo Scientific version 5.9) was used, and the assignment of signals was made based on the literature reports and the standards database of the National Institute of Standards and Technology (NIST).

2.3.2 Characterization of Crystalline Phases by X-Ray Diffraction

The mineralogical composition of PM_{2.5} was determined through XRD by using a PANalytical Empyrean X-ray diffractometer with Cu radiation ($K\alpha = 1.5405 \text{ \AA}$), and an X'Celerator ultra-fast

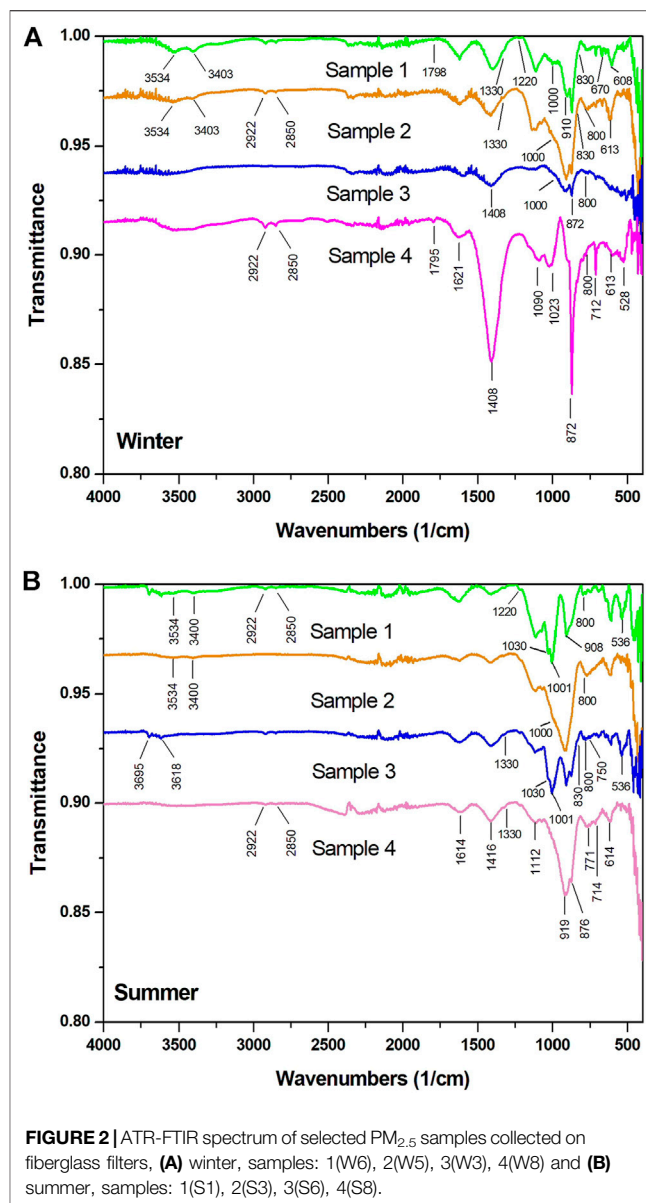


detector based on real-time multiple-step technology with Bragg-Brentano geometry. The diffractometer (operating at 45 kV and 40 mA) collected the scans in the 2θ range of 5° – 90° with a step size of 0.016° and 59 s per step. For structural refinements, both the Rietveld method and the crystalline phase identification approach were performed by using the High Score Plus software version 3.0.5 and the ICDD PDF+4 plus database as well (ICDD, International Center for Diffraction Data, Newtown Square, PA, United States).

3 RESULTS AND DISCUSSION

3.1 PM_{2.5} in the Monterrey Metropolitan Area During the Winter and Summer Seasons

The daily variation of PM_{2.5} concentrations found in the MMA during the two study periods is shown in **Figure 1**. The average concentrations of PM_{2.5} in winter were much higher (three times higher) than in summer. The concentrations found in winter and summer were 84.39 ± 11.67 and 25.04 ± 3.05 $\mu\text{g}/\text{m}^3$, respectively. A similar seasonal trend has been observed in other studies, which were conducted in different cities (Zhou et al., 2020; Duan et al., 2021). According to the regulation by Mexican Norm NOM-025-SSA1-2014 (SSA, 2014), the maximum allowed limit of PM_{2.5} in the air is 45 $\mu\text{g}/\text{m}^3$ (24 h average). Therefore, the levels found in the winter samples from the San Bernabé station was above the maximum allowed limit, suggesting the poor air quality and potential health risk to the exposed population. The high levels found during the winter season was attributed to the increase in both fossil fuels and biomass burning, which was from the high energy demands by both industries and residences during this season. Similar



results have been reported by different researchers (Ravindra et al., 2022; Wang et al., 2022). In addition, low wind speeds and rainfalls were registered during the winter (**Table 1**). These conditions favored the stagnation of particles in the area.

3.2. Functional Groups, Light-Absorbing and Fluorescent Properties of PM_{2.5}

3.2.1 Identification of Chemical Functional Groups by ATR-FTIR

The infrared spectra of the PM_{2.5} samples that were collected in winter and summer are shown in **Figure 2**. In the two study period, the absorption bands between 612 and 615 cm^{-1} and $1,080$ and $1,135$ cm^{-1} was attributed to the sulfate ions, which

TABLE 2 | Summary of the functional groups identified by FT-IR on the PM_{2.5} samples collected in both seasons.

Functional group	Wavelength (cm ⁻¹)	Winter samples	Summer samples
Sulfate	613, 1,080–1,135	ALL	ALL
Nitrate	820–830, 1,320–1,330, 1,760–1,800	W4, W5, W6, W8	S5, S6, S7, S8
Si-O	800, 1,000–1,044	W1, W2, W3, W5, W6, W7, W8	S1, S2, S3, S6, S7, S8
Al-OH	900–920, 3,618–3,700	W5, W6, W7	S1, S3, S6, S8
Carbonate ions CO ₃ ²⁻	712, 872, 1,412	ALL	ALL
Aromatic	772, 870, 910, 1,030,	ALL	ALL
OH stretching (water and/or hydroxylated compounds such as alcohols, polyols)	1,617, 1,640, 3,400	W1, W2, W4, W5, W6, W8	ALL
Aliphatic stretching	2,850, 2,920	W1, W2, W4, W5, W6, W7, W8	S1, S2, S4, S5, S6, S7, S8
O-H groups associated with alcohols, phenols, and carboxylic acids	3,534, 3,560	W1, W2, W4, W5, W6 W8	S1, S3, S5, S6, S7, S8
Carbonyl	1,798–1,800	W4, W6	S6, S7, S8

were likely as CaSO₄ (Allen et al., 1994; Maria et al., 2002; Radulescu et al., 2017; Yu et al., 2018; Zeb et al., 2018). It is of further importance to notice that CaSO₄ particles has a cooling effect on the atmosphere, which causes a negative radiative forcing and alters the troposphere temperature balance (Buseck and Pósfai, 1999; Martin et al., 2004). A summary of the chemical species that were found in the samples is found in **Table 2**. In majority of the collected samples, CO₃²⁻ signals (i.e., at 1,412 cm⁻¹ and 872 cm⁻¹) were predominant in the PM_{2.5} samples (Shaka' and Saliba, 2004; Bahadur et al., 2010; Siciliano et al., 2018). Moreover, the band found between 710 and 719 cm⁻¹ was related to the asymmetric vibrations of CaCO₃ (Varrica et al., 2019). Recent studies indicated that both carbonate ion and its products from atmospheric aging can affect the climate directly by dispersing and absorbing solar and terrestrial radiation (Crowley et al., 2010; Tang et al., 2015). They can affect the climate indirectly by changing the microphysics, albedo, and useful life of clouds.

The weak shoulder signals between the ranges from 1,320 to 1,330 cm⁻¹ and 820–830 cm⁻¹ in some samples suggested the presence of NO₃⁻ species (**Figure 2B**). These signals overlapped with the strong CO₃²⁻ signals between 1,412 and 870 cm⁻¹. In addition, in some summer and winter samples, the absorption signals between 1,760 and 1,800 cm⁻¹ were observed, which indicated the presence of inorganic nitrate. Previous studies on the MMA have reported the presence of NO₃⁻ in PM_{2.5} (Martinez et al., 2012; Mancilla et al., 2019). Meanwhile, the peaks between 1,000 and 1,044 cm⁻¹ and peak at 800 cm⁻¹ were due to Si-O bonds (samples: S1, S3, S6, W6, W5, and W3). The peak between 1,000 and 1,044 cm⁻¹ was due to the asymmetric stretching vibrations of the O-Si-O, while the peak at 800 cm⁻¹ was due to bending vibrations of the O-Si-O bond in the silicates (Maria et al., 2002; Shaka' and Saliba, 2004; Simonsen et al., 2009; Radulescu et al., 2017; Zeb et al., 2018). In addition, in both summer and winter samples, a peak was observed between 900 and 920 cm⁻¹, which was indicative of Al-(OH) bond vibrations. Compounds with Al-(OH) are usually present in aluminosilicate minerals such as kaolinite (Al₂Si₂O₅(OH)₄) (Ravisankar et al., 2010). It

should be noted that this peak appeared more intense in the summer samples and in some cases this peak overlapped with the carbonate band at ~877 cm⁻¹. The absorption signals found between 3,618 and 3,700 cm⁻¹ as well as 3,695 and 3,700 cm⁻¹ corresponded to the vibrations of the OH functional groups, which are typically located between the tetrahedral and octahedral layers of clay minerals (aluminosilicates). These functional groups have been shown to interact with the Si-O-Si layers to produce bonds, which produce characteristic absorptions at 3,620 and 3,695 cm⁻¹ (Davarcioğlu, 2011; Varrica et al., 2019). Additionally, the absorption bands at lower frequencies of around 540 cm⁻¹ and the small peak at 750 cm⁻¹, which appeared in some samples were attributed to the Al-O-Si bonds in silicates (Chou et al., 2005; Coury and Dillner, 2008).

The OH stretching vibrations around 3,400 cm⁻¹ observed in our samples (**Figure 2**) indicated the presence of water and/or hydroxylated compounds such as alcohols and polyols from biogenic sources and biomass burning (Gipson et al., 2015; Siciliano et al., 2018; Zapata-Hernandez et al., 2020). The broad band observed between 1,617 and 1,640 cm⁻¹ confirmed the presence of water in the samples. The broad band signal between 1,617 and 1,640 cm⁻¹ indicated of an overlap of the signals from different chemical functional groups including the stretching vibration absorptions for C=C aromatic and C=O bonds. Some authors have attributed this broad band signal to the functional groups found in organonitrates, aromatic amides, and organic amines (Ji et al., 2015; Radulescu et al., 2017; Siciliano et al., 2018; Zapata-Hernandez et al., 2020). Meanwhile, the appearance of the weak shoulder signals at around 1,220 cm⁻¹ in most of the samples supported the presence of organ nitrated compounds (Shaka' and Saliba, 2004).

The broad band observed between 3,534 and 3,560 cm⁻¹ in our samples (**Figure 2**) were due to the vibrations of the O-H groups in alcohols, phenols, and carboxylic acids (Allen et al., 1994; Coury and Dillner, 2008; Shaka' and Saliba, 2004). A weak peak between 1,798 and 1,800 cm⁻¹ was observed in three and five of the summer and winter samples, respectively. This

peak corresponded to the vibrations of the carbonyl functional group (C=O) in carboxylic acids. The amounts of carboxylic acids seemed to be higher in the winter samples suggested in **Figure 2A** (Siciliano et al., 2018). In most of the collected samples, peaks were observed between 2,920 and 2,850 cm^{-1} , which were associated to the CH_2 in aliphatic compounds (Shaka' and Saliba, 2004; Zapata-Hernández et al., 2020).

3.2.2 Analysis of PM_{2.5} Samples by X-Ray Diffraction and X-Ray Photoelectron Spectroscopy

3.2.2.1 Chemical Analysis of the Crystalline Phases by X-Ray Diffraction

The XRD diffractograms obtained for the PM_{2.5} samples in the two study periods are shown in **Figure 3**. Several reflections with different intensities were observed in the diffractograms. Most of the signals corresponded to the crystalline phases of CaCO_3 (index number or ICDD No. 010721937), SiO_2 (ICDD No. 010781252), and $\text{CaSO}_4 \cdot 2\text{H}_2\text{O}$ (ICDD No. 010741433). Signals

with lower intensities corresponded to the aluminosilicates including kyanite (ICDD No. 000110046), albite (ICDD No. 010831658), leucite (ICDD No. 010768736), sillimanite (ICDD No. 000380471), pyrophyllite dehydroxylated (ICDD No. 010734051), and NaCl (ICDD No. 010763457). In the literature it is reported that in the study region there are some mineral deposits related to these crystalline phases (such as muscovite, sillimanite, kaolin, albite, quartz, plagioclase, feldspars, and micas), only some of them are commercially exploited (nl.gob.mx, 2020). On the other hand, it is known that these mineral phases are used in the refractory and ceramic industry, which are abundant in the area and therefore it is not ruled out that they also contribute to the emission of these crystalline compounds (Bradt, 2008). Adjustments on the reflection profiles were carried out by the Rietveld method, which allowed us to perform semiquantitative analysis on each of the crystalline phases detected (Rietveld, 1969). The refinement of the signals provided the mass percentage of each crystalline phase in the diffractograms. The results showed that the most abundant crystalline phases were CaCO_3 and SiO_2 (**Table 3**). CaSO_4 was also abundant while aluminosilicates and NaCl were the least abundant. These phases have been extensively reported in the literature (Ahmady-birgani et al., 2015; Zarasvandi et al., 2011). The average percentage of CaCO_3 was slightly higher in summer (73.9%) than in winter (71.1%). These findings were consistent with the ATR-FTIR results, which showed the carbonate absorption bands at 1,412, 872, and 710–719 cm^{-1} , in all samples collected in both seasonal periods. These crystalline phases may have emerged from natural sources (resuspension of crust material) and anthropogenic sources. We note that MMA is a semiarid region with many ceramic, glass and, cement industrial facilities, as well as quarries inserted within the expanding metropolitan area.

On the other hand, the average percentage of CaSO_4 found was significantly higher in winter (10.2%; min: 0% and max: 30%) than in summer (4.5%; min: 0% and max: 12%), which was consistent with the findings by the ATR-FTIR technique. In ATR-FTIR, we found more frequent and greater intensity signals for SO_4^{2-} (1,080–1,135 and 612–615 cm^{-1}) in the winter samples. This finding is relevant as most of the previous studies in the MMA have assumed that sulfate associated to the PM_{2.5} is mainly in the form of $(\text{NH}_4)_2\text{SO}_4$ (Martinez et al., 2012; Mancilla et al., 2019). The higher percentage of CaSO_4 found in the winter samples is likely more related to the meteorological parameters and concentration of SO_2 in the atmosphere, since we have

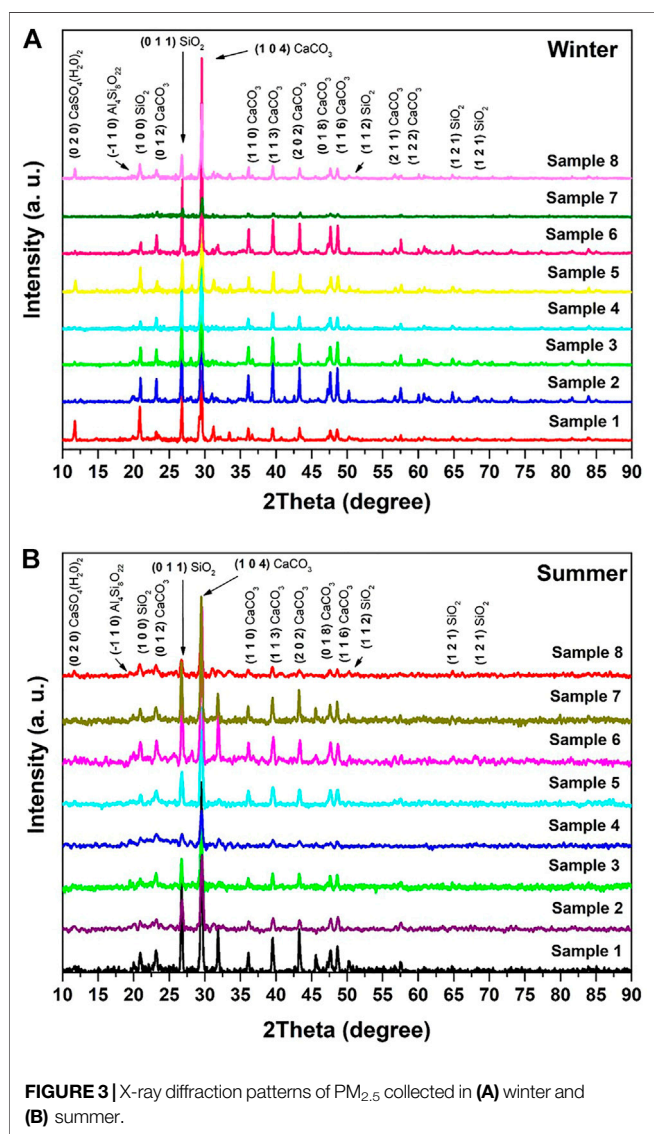
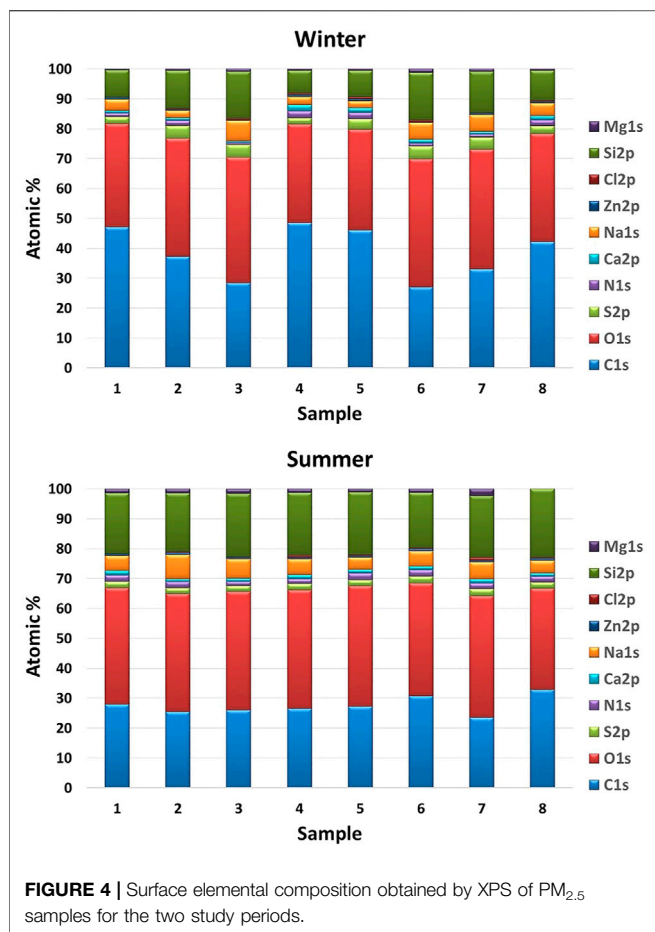


TABLE 3 | Contents of the most important crystalline mineral phases present in the PM_{2.5} samples, which were obtained by x-ray powder diffractometry.

% Phases	Season	
	Summer	Winter
Calcite	73.9	71.1
Quartz	16.9	15.2
Gypsum	4.5	10.2
Aluminosilicates	3.4	3.2
Halite	1.2	0.3



considered CaSO₄ as a phase of secondary origin. Sulfates are formed by photochemical reactions that occur between their main precursor (SO₂) and oxidizing species such as O₃ and NO_x (Xu et al., 2016). Unfortunately, SO₂ is not monitored in the San Bernabé station. However, further exploration of available ground-level SO₂ data from the local air quality monitoring network resulted in identifying that the nearby North 2 station had a complete dataset for the periods of interest. The North 2 station is approximately 6 km to the southeast of the Northwest (San Bernabé) station, in a very similar landuse and main emission sources setup. Assuming that the North 2 station is a good proxy for the Northwest station, we retrieved SO₂ data for the North 2 station for the months of interest (**Supplementary Table S2**). The data confirms that SO₂ levels are higher during the winter period, which could contribute to the formation of sulfates in this season. Another factor to consider is the changes in the meteorological parameters, where several studies have shown the dependency of sulfate levels to relative humidity and wind speed (Banerjee et al., 2015; Pant et al., 2015; Lu et al., 2016). For example, Song et al. (2014) attributed the high percentages of sulfate found in their PM₁₀ samples to the higher humidity and low wind speed in the collection/sampling area (Henan, China). Moreover, Yue et al. (2022) found that the reaction between SO₂ and CaCO₃ particles in the atmosphere was favored by relative humidity values of greater than 40%. Therefore, the low wind

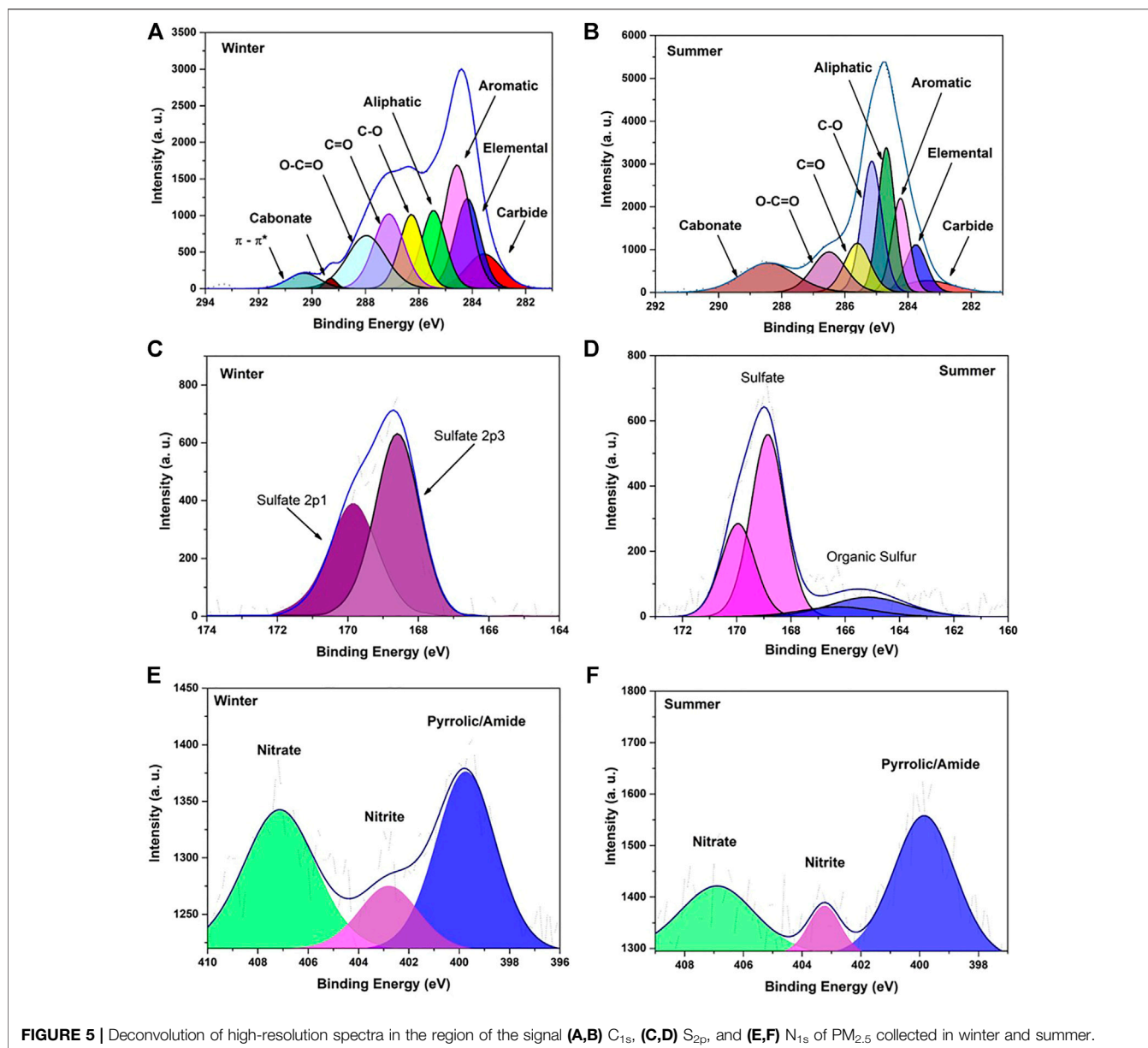
speed, high relative humidity, as well as the abundance of SO₂ y CaCO₃ during the winter sampling (**Table 1**) in the MMA explained the higher proportions of CaSO₄ found in the winter samples. It should be noted that there is no known primary source of CaSO₄ near the study area. In addition, in some samples it is not possible to detect the presence of this mineral phase, it is only detected when the meteorological parameters are favorable for the photochemical reaction to take place. For everything described above, it can be thought that the CaSO₄ found in the PM is of secondary origin

Similar amounts of SiO₂ were found in all the samples. Several reports have associated SiO₂ with natural sources (Adamo et al., 2008; Saitoh et al., 2008; Song et al., 2014). Thus, it was not surprising to find SiO₂ in our samples, since the overall soil composition of the MMA falls within a sandy profile with numerous deposits that are rich with SiO₂. Nonetheless, the contributions from anthropogenic sources were not overlooked. For example, there is a large glass industry in MMA, which uses crystalline SiO₂ as raw material. Finally, we note that the XRD and ATR-FTIR results of this investigation complemented each other.

3.2.2.2 Determination of Surface Elemental Composition by X-Ray Photoelectron Spectroscopy

High-resolution XPS spectra of the elements identified in the survey scan were corrected using the C_{1s} signal (285 eV) as reference. The assignment of signals was carried out by considering the data from the literature and National Institute of Standards and Technology (NIST) database. The atomic percentage of silicon was corrected by the method described by Atzei and Rossi (2004) and Gilham et al. (2008). In both winter and summer samples, high-intensity bands related to C and O was found along with low-intensity bands related to Si, Na, N, and S. Additional elements identified through their high- and low-resolution spectra were Ca, Mg, Zn, Cl, and F. The surface elemental composition of the PM_{2.5} samples are shown in **Figure 4**. The most abundant elements found were C, O, and Si followed by Na, S, N, and Ca. Similar results have been reported in studies by Guascito et al. (2015), Atzei et al. (2014) and Huertas et al. (2012). In these previous studies, C and O were the predominant elements found on the PM_{2.5} samples. The average percentage of C were higher in the winter sample, which can be attributed to the higher consumption of fossil fuels due to e.g., increased use of heating both at the industrial and residential level in the MMA (**Figure 4**).

Signal speciation of C, N, S, and Ca was performed by deconvolution of the high-resolution spectrum of each element. For example, consider the high-resolution spectra of C, N, and S shown in **Figure 5**. For C_{1s} (280–295 eV), the deconvolutions showed eight different states of oxidized carbon found in all samples. These were the aliphatic (C-C, 285 eV), aromatic (C=C, 284.7 eV), EC (284 eV), carbonyl (C=O, 288 eV), carbides (283.6 eV), carboxylics (O-C=O, 289 eV), carbonates (289.5 eV), and ether/alcohol (C-O, 296.5 eV). Several researchers have reported these contributing functional groups on PM (Gaddam and Vander Wal, 2013; Atzei et al., 2014). The atomic percentages of each contributing



functional group to the C_{1s} signal are summarized in **Table 4**. The aromatic hydrocarbons in all the samples were considered as the highest component to the C_{1s} signals. This was followed by the EC and aliphatic hydrocarbons chains. The least contributing component in the winter and summer samples were carbonates and carbides, respectively. The atomic percentages of highly oxidized species such as ether, alcohol, carboxylic acids and/or carbonyl groups were significantly higher in the winter samples. These were consistent with the results of the ATR-FTIR spectra. The higher proportion of these functional groups in winter could be related to an increase in coal burning, in addition to a greater atmospheric oxidation caused by changes in meteorological parameters (Domínguez et al., 1999; Ahlers et al., 2000; Siciliano et al., 2018). In contrast, the decrease in oxidized species observed in summer could explain the higher

proportion of aromatic and aliphatic groups recorded in this season. On the other hand, average area percentage of EC in all samples did not show any significant variation.

For the observed N_{1s} signal in the samples, three contributors were identified including amide/pyrrole groups, nitrites, and nitrates, positioned at bonding energies of 399.2 and 402 eV and 407, respectively. The results obtained for the winter and summer samples showed a similar trend, where amide/pyrrole groups predominated at the surface level on PM_{2.5} followed by nitrates and nitrites. These were consistent with the ATR-FTIR findings where organic amides and amines, as well as inorganic nitrate were found in the samples. The abundance of amide/pyrrole groups was associated to the burning of fossil fuels. The nitrates and nitrites were of secondary origin from the photo-oxidation reactions of gaseous nitrogenous precursors in the

TABLE 4 | Atomic percentage of each contributing functional group to the C_{1s} signals (*n* = 8).

Sample	Element (atomic %)							
	Carbide	Elemental	Aromatic C-H	Aliphatic C-H	C-O	C=O	O-C=O	Carbonate
Winter samples								
1	0.1	13.7	23.7	20.6	17.4	17.0	5.7	1.9
2	6.2	21.9	19.7	16.3	14.2	14.2	2.0	5.5
3	7.9	14.7	24.8	12.4	11.5	14.7	13.4	0.8
4	13.4	20.1	10.3	16.7	12.5	13.5	8.3	5.3
5	14.2	21.6	14.5	13.3	13.6	15.1	4.8	2.9
6	0.1	24.8	22.6	23.1	19.7	5.0	3.1	1.6
7	14.0	29.8	22.1	15.3	8.9	6.2	2.5	1.3
8	0.1	22.3	35.5	14.7	7.9	16.3	3.0	0.2
Summer samples								
1	2.7	21.7	25.1	26.7	10.3	5.6	6.6	1.4
2	0.5	22.1	19.5	20.5	8.4	14.7	13.1	1.3
3	1.3	13.1	28.9	25.5	18.8	3.8	5.4	3.1
4	4.7	13.6	42.6	11.9	15.0	—	—	12.2
5	—	17.6	40.8	18.7	7.1	6.5	1.6	7.7
6	15.8	22.9	22.8	15.7	13.8	—	—	9.0
7	—	20.2	27.8	19.7	12.7	5.9	—	13.7
8	—	36.9	26.0	27.0	—	—	—	10.2

atmosphere. In the literature, it has been reported that some ions of secondary origin, such as nitrites, are more stable under conditions of low solar radiation, which is consistent with the lower solar radiation recorded in winter (Paoletti et al., 2003). The atomic percentages obtained for the amide/pyrrole groups and nitrates in the two seasons were similar. This confirmed that seasonal variation had no significant effect on the amounts of these species in the atmosphere. Interestingly, the concentrations of nitrite were significantly higher in the winter samples (Table 5), which was attributed to the typically lower solar radiation during the cold months (Hoek et al., 1996; Lee et al., 1999; Paoletti et al., 2003).

Two components for the Ca_{2p} signal were identified, where one was located at a binding energy of 347 eV, which corresponded to CaCO₃. The other was at 347.8 eV, which was associated with CaSO₄ (Guascito et al., 2015). Our results showed that CaCO₃ was the main signal contributor in all samples, while the highest percentages of CaCO₃ were found in the summer samples (e.g., 74.6%). Notably, the deconvolution of the C_{1s} signals suggested a higher percentage of CaCO₃ in the summer samples. This was explained by the summer activities related to the extraction of limestone from local quarries and its use as a raw material in the cement binder industry. The deconvolution of S_{2p} signals showed that the sulfates and organic sulfur compounds dominated the winter (68.4%) and summer (65.9%) samples, respectively. The higher levels of CaSO₄ found in the winter samples were related to the changes in meteorological conditions and possibly higher concentrations of SO₂ in the atmosphere during the sampling. In summer, the meteorological conditions did not favor the formation of the CaSO₄, which led to an increase in the percentages of organic sulfur in this season.

3.2.3 Diffuse Reflectance Spectroscopy Analysis

The DRS technique has been widely used for the characterization of solid materials (Zwinkels et al., 2014; Bock et al., 2019), since it is a tool useful to determine the electronic transitions from the valence to conduction band (band gap) of semiconductor oxide powders (Escobedo-Morales et al., 2019). In the environmental sciences, has been applied mainly for the analysis of minerals in soils (Sellitto et al., 2009; Szalai et al., 2013), however, we have found a few studies that used DRS for the characterization of atmospheric particulate material. For example, Wonaschütz et al. (2009) used this technique for the characterization of BC and BrC in atmospheric aerosols. In another study, Morozzi et al. (2021) used DRS to characterize the diverse mineral phases of the Sahara dust that were present in the PM samples obtained from the Mediterranean area.

The diffuse reflectance spectra obtained from the PM_{2.5} samples are shown in Figures 6A,B. Significant attenuation of the signal response in the visible region (400–800 nm) were observed in all the spectra, indicating the presence of chromophores that were likely from the carbonaceous materials in the samples. On the other hand, the UV region spectra showed some noticeable changes in the slopes of the curves. These were associated to the electronic transitions in the inorganic materials present in the samples (Makuła et al., 2018). The spectra were converted by the Kubelka–Munk function. To better define the processes involved, the second derivative was obtained by following the methodology proposed by Torrent and Barrón (2015) and the results are shown in Figures 6C,D. In the spectra, the absorption band near 250 nm was related to the presence of CaSO₄, whose absorption range was previously reported to be between 250 and 350 nm (Nagabhushana et al., 2010). The absorption band

TABLE 5 | Atomic percentage of each contributing functional group to the (a) N_{1s}, (b) Ca_{2p}, and (c) S_{2p} signals.

Sample	N _{1s}					
	Winter			Summer		
	Atomic %			Atomic %		
	Pyrrolic/Amide	Nitrite	Nitrate	Pyrrolic/Amide	Nitrite	Nitrate
1	29.0	50.6	20.5	66.0	-	34.0
2	60.9	24.5	14.6	57.2	10.1	32.7
3	53.2	27.4	19.3	65.1	0.0	34.9
4	66.3	—	33.7	55.1	11.9	33.0
5	48.9	29.8	21.3	72.8	—	27.2
6	71.7	13.3	15.0	62.7	8.7	28.6
7	44.1	15.7	40.3	49.8	21.8	28.4
8	50.6	14.4	50.6	48.1	41.1	10.9

Sample	Ca _{2p}			
	Winter		Summer	
	Atomic %		Atomic %	
	Carbonate	Sulfate	Carbonate	Sulfate
1	41.0	59.0	87.6	12.4
2	48.7	51.3	68.1	31.9
3	51.3	48.8	72.3	27.7
4	48.2	51.8	72.9	27.1
5	53.5	46.6	79.7	20.3
6	39.4	60.6	76.3	23.7
7	34.4	65.6	72.2	27.8
8	83.9	16.1	67.7	32.3

Sample	S _{2p}			
	Winter		Summer	
	Atomic %		Atomic %	
	Sulfate	Organic sulfur	Sulfate	Organic sulfur
1	80.0	20.0	29.5	70.5
2	74.7	25.3	100.0	—
3	57.4	42.6	20.3	79.7
4	72.1	27.9	27.3	72.8
5	92.8	7.2	21.9	78.1
6	56.2	43.8	19.9	80.1
7	58.2	41.8	23.9	76.1
8	55.7	44.3	29.7	70.3

between 210 and 230 nm corresponded to the CaCO₃ electronic transition from the valence to conduction band (Al Omari et al., 2016). The additional absorptions observed between 330–400 nm in some samples are possibly related to electronic transitions of the aluminosilicates containing transition metals (Zent et al., 2008; Tarantola et al., 2019). The above demonstrates the application of the DRS technique to characterize the inorganic fraction present in PM. In addition, it is versatile, simple and low cost since the analysis of the sample is done directly in the filter, without the need to use reagents or solvents for its

3.2.3.1 UV-Vis Analyses of Water-Soluble Organic Carbon

To fully understand the optical properties of the water-soluble fraction, UV-Vis analyses were performed on the aqueous extracts of the PM_{2.5} samples collected in the San Bernabé monitoring station. The variation of the Abs_λ with respect to

the wavelength of radiation in the range of 300–600 nm is shown in **Figure 7A**. In both seasons studied, the absorption intensities decreased notably at longer wavelengths, suggesting a strong dependence with the radiation wavelength, which is characteristic of BrC (Cheng et al., 2016; Wu et al., 2020). Furthermore, the absorption coefficients of the winter samples were higher than the summer samples. Similar results have been reported by Chen et al. (2018) for samples obtained in Nanjing, China. Prior studies have associated the Abs₃₆₅ with the absorption coefficient of BrC (not inorganic salts) (Hecobian et al., 2010). The values for Abs₃₆₅ and temporal variation are shown in **Table 6** and **Figure 7B**, respectively. The Abs₃₆₅ values were higher in the winter ($1.15 \pm 0.49 \text{ Mm}^{-1}$) than summer ($0.66 \pm 0.19 \text{ Mm}^{-1}$) samples, which has been a seasonal trend confirmed by other researchers (Kim et al., 2016; Chen et al., 2020). The values we found were comparable to those reported by

Liu et al. (2018) for samples obtained in Guangzhou City, China, and by Liu et al. (2013) in Atlanta, United States. However, our values were lower than those reported by Satish et al. (2017) for samples obtained from the cities of Indo-Gangeti Plain, India Satish et al. (2017) and Huang et al. (2018) for samples obtained from Xi'an, China. Strong correlations of the Abs_{365} of water extracts with WSOC concentrations for both winter ($r = 0.89$) and summer ($r = 0.93$) were found (Figure 7C), which is indicative that WSOC contains BrC (Chen et al., 2020). The difference in the Abs_{365} values found in both seasons could be attributed to differences in the emission sources that predominate in each season (Chen et al., 2018; Zhan et al., 2022).

On the other hand, the average MAE_{365} values in the winter and summer samples were $0.23 \pm 0.05 \text{ m}^2 \text{ g}^{-1}$ and $0.19 \pm 0.04 \text{ m}^2 \text{ g}^{-1}$, respectively (Table 6 and Figure 8A). These results indicate that BrC in winter has a higher absorption capacity compared to summer. This could be attributed to a higher concentration of BrC chromophores in winter and/or to differences in the chemical nature of chromophores that predominate in the cold season as a result of differences in emission sources. In this study, the observed MAE_{365} values were lower than those reported for cities with higher pollution indices such as Beijing, China (Yan et al., 2015), Xi'an, China (Yuan et al., 2020), and New Delhi, India (Kirillova et al., 2014).

In addition, our values were closer to the values reported for Seoul, Korea (Kim et al., 2016) and Atlanta, United States (Hecobian et al., 2010).

The AAE is a very important parameter that provides information on the spectral dependence of the aerosol and the absorption of light in bulk (e.g., extracts) (Moosmüller et al., 2011). In the literature, it has been reported that BC from the burning of fossil fuels generally has AAE values that were close to 1 (Fraund et al., 2020). This means that the refractive index values of BC are independent of the wavelength. AAE values slightly higher than one indicated the presence of BC or a mixture of BrC and BC (Pokhrel et al., 2017). Meanwhile, high AAE values between 5 and 9 revealed the predominance of BrC in the aerosol samples (Chakraborty et al., 2016; Lin et al., 2017). The AAE values calculated for WSOC of our samples in the wavelength range from 300 to 600 nm are summarized in Table 6. The average values obtained for the winter and summer samples were 6.32 ± 0.78 and 7.33 ± 1.02 , respectively (Figure 8B). The high AAE values in all samples as well as the high correlations found between Abs_{365} and WSOC concentration demonstrated an important contribution of BrC chromophores in the WSOC (Lin et al., 2017; Yuan et al., 2020). The AAE

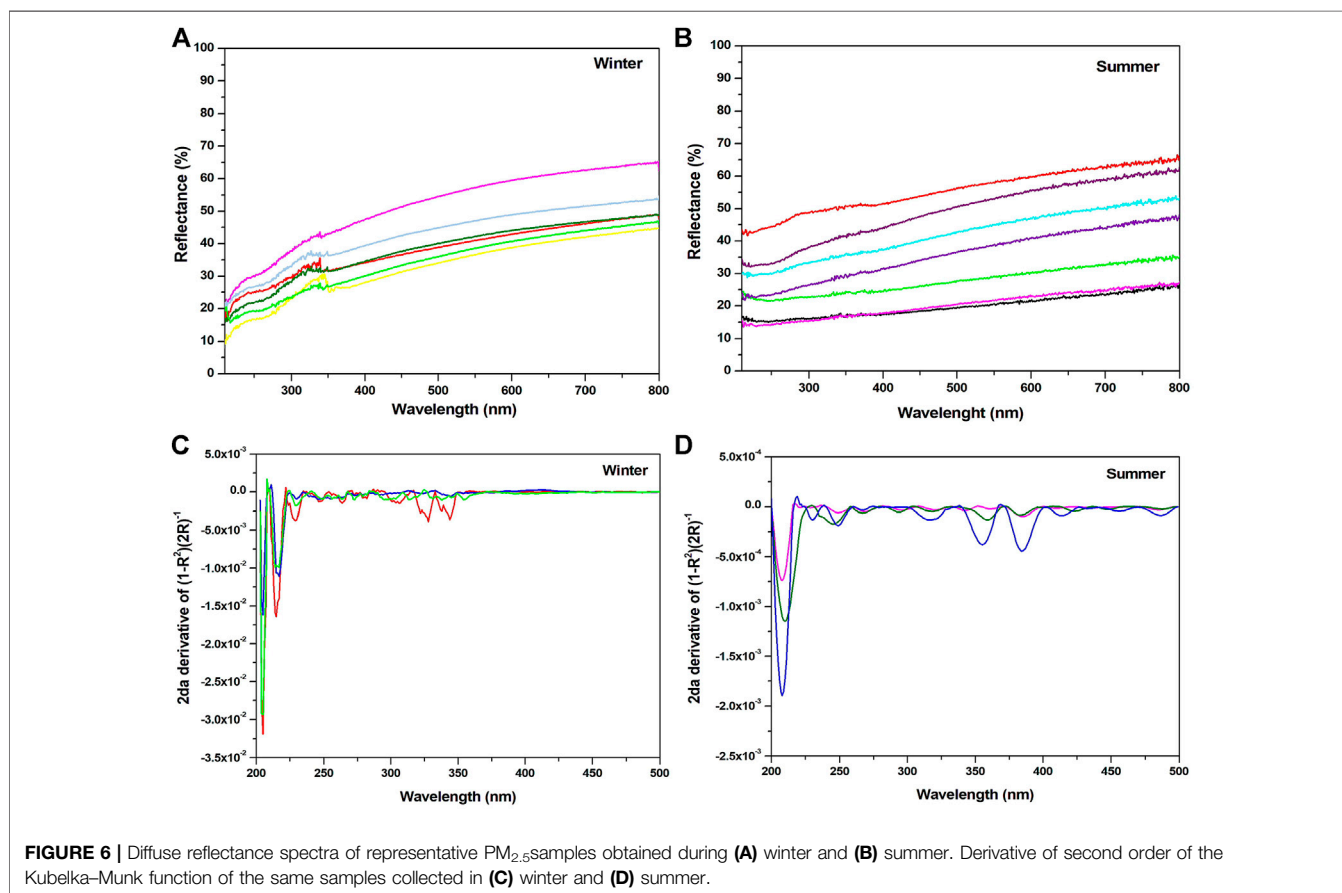
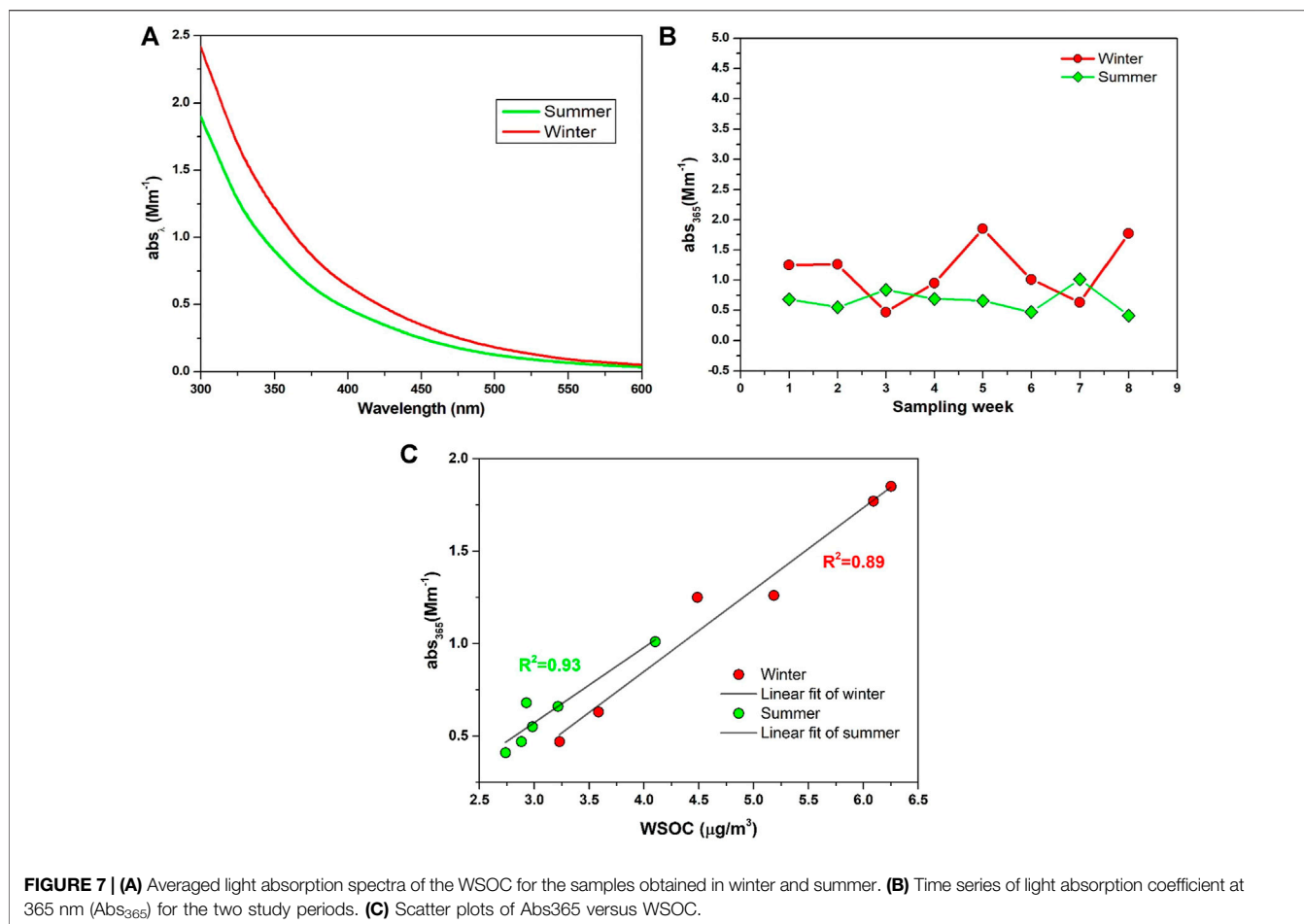


FIGURE 6 | Diffuse reflectance spectra of representative PM_{2.5} samples obtained during (A) winter and (B) summer. Derivative of second order of the Kubelka-Munk function of the same samples collected in (C) winter and (D) summer.



values were higher in the summer samples, indicating a greater contribution of compounds that absorb at shorter wavelengths in these samples. Similarly, Chen et al. (2018) reported that the highest and lowest values of AAE for PM_{2.5} samples collected throughout the year from Nanjing, China was obtained from the summer and winter samples, respectively. The results were explained by the difference in the chemical composition or emission sources in these seasons. Likewise, Kim et al. (2016) reported a similar seasonal variation, where the higher values of AAE in summer was attributed to the presence of metals that come from the Earth's crust

3.2.4 Analysis of PM_{2.5} by Fluorescence Spectroscopy

The fluorescence emission spectra (with excitation at 355 nm) of the filters collected during winter and summer are shown in **Supplementary Figure S1**. The maximum wavelength intensity of the spectra from the winter and summer samples ranged from 440 to 464 nm and 439–449 nm, respectively. Similar ranges have been reported by other researchers for highly oxygenated carbonaceous and humic-like substances (HULIS) (McKnight et al., 2001; Chen et al., 2016b; Qin et al., 2021). Barsotti et al. (2016) reported that HULIS derived from the oligomerization of phenolic compounds exhibited a strong fluorescence emission in

the vicinity of 450 nm. On the other hand, it is known that ozone and hydroxyl radicals are able to cause the oxidation of volatile organic compounds (VOCs) such as limonene and α -pinene. The oxidation generated HULIS that showed strong fluorescence emissions within the range of 437–513 nm. The average of maximum emission intensities was higher in the winter ($1.6 \times 10^6 \pm 7.8 \times 10^5$ a.u.) than summers ($1.4 \times 10^6 \pm 6.3 \times 10^5$ a.u.) samples. This was attributed to the greater amounts of oxygenated carbonaceous species found in the winter samples. Through XPS analyses, we also found slightly higher values for the total percentage of carbon and extent of functionalization by oxidized species on the C_{1s} signal in the winter samples.

An exploratory EEM study was conducted to gain insights on the fluorescent compounds found in the samples. The aqueous extracts of the samples obtained during both seasons were used. The fluorescence indexes HIX, BIX, and FI were determined. These indexes have been implemented in studies involving DOM in both soil and aquatic systems and aerosol due to the similarities in the optical aspects of WSOC and aquatic DOM. Indeed, these indexes have been shown to provide some information on the nature of the organic compounds present in the water-soluble fraction of aerosols (McKnight et al., 2001; Huguet et al., 2009; Birdwell and Engel, 2010). The FI values are summarized in **Supplementary Table S1**, where 40% of the samples showed FI ~

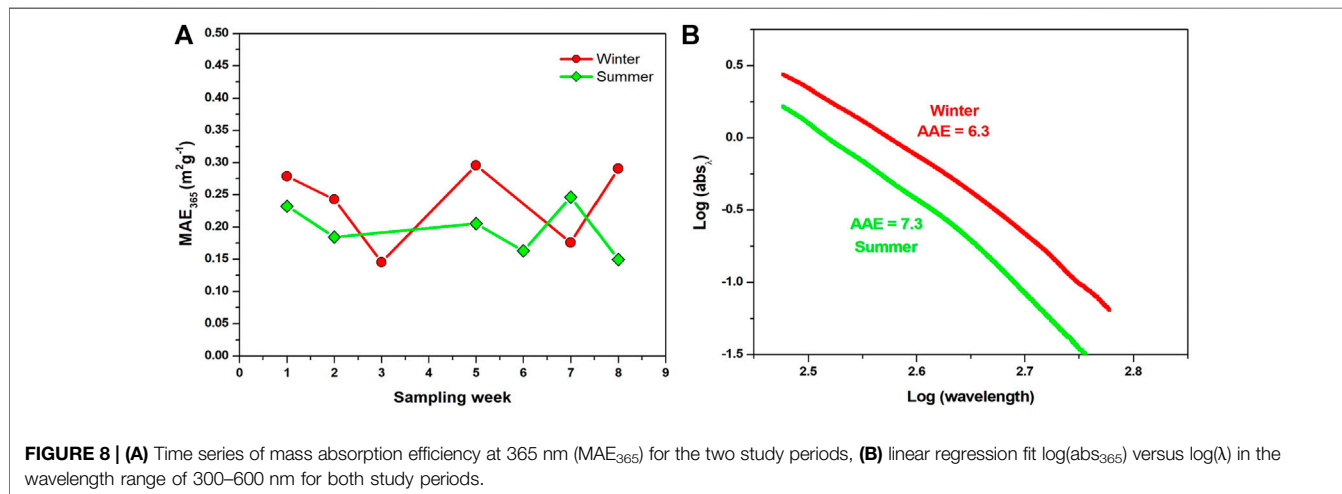
TABLE 6 | WSOC mass concentration and light absorption parameters (Abs_{365} , MAE_{365} , and AAE), measured during winter and summer in the two study periods.

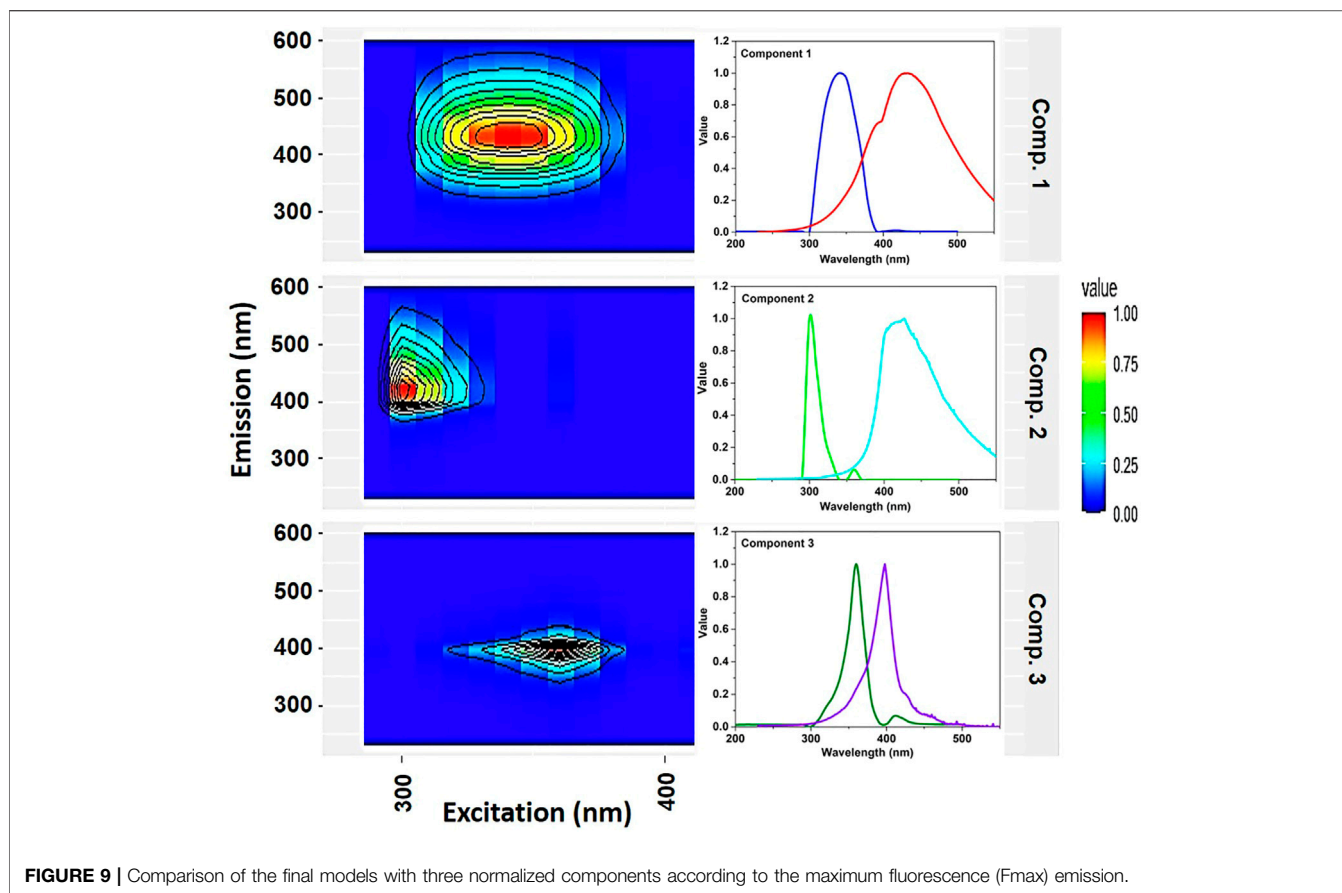
Sample	Winter				Sample	Summer			
	Abs_{365}	AAE	WSOC	MAE_{365}		Abs_{365}	AAE	WSOC	MAE_{365}
	Mm^{-1}		$\mu g/m^3$	$m^2 g^{-1}$		Mm^{-1}		$\mu g/m^3$	$m^2 g^{-1}$
1	1.25	6.93	4.49	0.28	1	0.68	7.23	2.93	0.23
2	1.26	5.36	5.18	0.24	2	0.55	7.59	2.98	0.18
3	0.47	6.72	3.23	0.15	3	0.84	5.69	—	—
4	0.95	6.06	—	—	4	0.69	6.10	—	—
5	1.85	5.06	6.25	0.30	5	0.66	7.96	3.22	0.21
6	1.01	6.31	—	—	6	0.47	8.49	2.88	0.16
7	0.63	6.99	3.58	0.18	7	1.01	7.11	4.10	0.25
8	1.77	7.14	6.09	0.29	8	0.41	8.43	2.74	0.15

1.5 values. This suggested the presence of fulvic acid-like substances with high aromaticity and of terrestrial origin. Meanwhile, 60% of the remaining samples produced FI values >2. This indicated the strong presence of fluorescent compounds with low aromaticity and of microbial origin. Similar results have been reported by Lee et al. (2013) in their EEM analysis of fresh and aged organic aerosols. They suggested that aerosols with FI values near 1.4 and 1.9 were associated with fulvic acids of terrestrial and microbial origin, respectively. The presence of this acid in our samples was verified by the FTIR and XPS results, where C = O ($1798-1800\text{ cm}^{-1}$) and OH ($3500-3650\text{ cm}^{-1}$) vibrations for the carboxylic acid group and OC = O, 289 eV to the C_{1s} signal for the carboxyl group, respectively were observed. The autochthonous contribution index value (BIX near 0.4) also suggested that fulvic acid came from nonbiological sources. In addition, the HIX index found in the aerosols of ~0.6 can be associated with the low-grade humification fluorescent components.

The PARAFAC model was applied to identify the possible sources of emission for the water-soluble carbonaceous substances that were present in the collected samples (Murphy et al., 2013). Recently, this model has been used to characterize the water-soluble organic matter in atmospheric aerosols (Mladenov et al., 2011; Matos et al., 2015; Chen et al., 2021) and organic matter in various aqueous matrices

(Ishii and Boyer, 2012; Dittmar and Stubbins, 2014; Wünsch and Murphy, 2021). It is important to mention that in Mexico and possibly in Latin America, fluorescence indices and the PARAFAC model had not yet been used in the study of atmospheric aerosols. The results obtained are shown in Figure 9. The model was fixed for three components and helped determine 99.1% the data set variance and delivered central consistency values higher than 87%. Additionally, the model was validated through the analysis of divided halves (Supplementary Figure S2) and Tucker's congruence coefficient for both excitation and emission spectra. The coefficients were found to be higher than the similarity threshold (0.95) proposed by Murphy et al. (2014). Component 1 (C1) revealed the primary and secondary signals ($\lambda_{ex}/\lambda_{em}$) of 340/433 nm and 340/394 nm, respectively. Component (C2) gave the primary and secondary signals of 300/410 nm and 360/410 nm, respectively. Component 3 (C3) showed one signal of 360/398 nm. The signals for C1 were similar to those reported for highly oxygenated HULIS of terrestrial and dust origin, which were found in aerosol samples from urban areas and organic matter dissolved in water samples (Fu et al., 2015; Yan and Kim, 2017; Qin et al., 2018; Wang et al., 2020). Moreover, Wen et al. (2021) applied the PARAFAC model to samples collected from three sites with different environments in northern China. One of the components presented signals of 245 and 360/476 nm, which were associated with highly oxygenated HULIS from terrestrial sources. In





addition, Murphy et al. (2011) attributed the signal of 349/431 nm to terrestrial humic- and fulvic-like fluorescent compounds in their samples of organic matter dissolved in water.

In the case of C2, the fluorescence was associated to HULIS of microbial origin (Søndergaard et al., 2003; Zhuo et al., 2010; Murphy et al., 2011). Similar fluorescent compounds have been identified in the DOM of groundwater (Chen et al., 2010). On the other hand, C3 was similar to those found for humic fluorophores present in wastewater (Stedmon and Markager, 2005; D'Andrilli et al., 2013). Here, the results of the PARAFAC study were fully consistent with those obtained from the fluorescence indices study. These studies revealed the contribution of HULIS of terrestrial and microbial origin in the samples. It is important to emphasize that the emission sources and chemical composition of the fluorophores in the PM may not be the same as those found in the DOM. Moreover, only a few studies have used the fluorescence indices and PARAFAC method to characterize the fluorophore components in PM samples. Therefore, it was not possible to compare the detected components that may be found in different sources of atmospheric aerosols, such as biomass burning, fossil sources, secondary aerosols of biogenic, and anthropogenic VOCs, among others. In this sense, the present work, although an exploratory study, may serve as a basis to deepen the study of the fluorophore components present in atmospheric aerosols in Mexico.

4 CONCLUSION

This study investigated the light absorption characteristics and chemical composition of PM_{2.5} particles and their water-soluble fraction. In winter, the concentration of PM_{2.5} recorded at the San Bernabé station exceeded the limits in Mexico (NOM-025-SSA1-2014), which was a potential health risk to the exposed population. The presence of inorganic species in the samples collected during winter and summer, such as CaCO₃, CaSO₄, SiO₂, and aluminosilicates were identified by ATR-FTIR, XRD, and XPS techniques. The DRS spectra showed that most of the detected constituents of the sample absorbed mainly in the UV region (200–350 nm). The highest percentages of CaSO₄ were found in the winter samples (both at the surface level and in the bulk). This was attributed to the higher concentration of SO₂ in the atmosphere, as well as the higher humidity and low wind speed that were recorded during the winter months of sample collection. The speciation of the C_{1s} signal showed eight different oxidation states for carbon in all samples, with aromatic hydrocarbons, EC, and aliphatic hydrocarbons as the main contributors to the overall signal.

The light absorption by the water extracts exhibited a strong dependence with the wavelengths in the ranges 300 and 600 nm. Optical parameters, such as Abs₃₆₅ and AAE, as well as the high correlation found between Abs₃₆₅ and WSOC, showed that a fraction of WSOC corresponds to BrC chromophores. The Abs₃₆₅

and MAE₃₆₅ were found to be higher in the winter than in summer samples. This was attributed to the differences in the chemical nature of the BrC compounds and/or to a higher concentration of these compounds in the winter samples. EEM-PARAFAC analysis showed that the water-soluble BrC compounds were mainly HULIS that come from terrestrial (C1), microbial origin (C2) and humic fluorophores (C3). A high correlation was found between the fluorescence indices (FI, HIX, and BIX) and EMM-PARAFAC, which suggested the importance of both approaches in establishing the possible sources of emission for the BrC compounds in the aqueous extracts. We believe that it is necessary to continue the global studies on the molecular characterization of BrC compounds and fluorescence properties of atmospheric WSOC. These studies will allow us to establish a database on atmospheric aerosols for more accurate identification of possible emission sources.

DATA AVAILABILITY STATEMENT

The original contributions presented in the study are included in the article/**Supplementary Material**, further inquiries can be directed to the corresponding author.

REFERENCES

- Adamo, P., Giordano, S., Naimo, D., and Bargagli, R. (2008). Geochemical Properties of Airborne Particulate Matter (PM10) Collected by Automatic Device and Biomonitoring in a Mediterranean Urban Environment. *Atmos. Environ.* 42, 346–357. doi:10.1016/j.atmosenv.2007.09.018
- Ahlers, F., Bubert, H., Steuernage, S., and Wiermann, R. (2000). The Nature of Oxygen in Sporopollenin from the Pollen of *Typha Angustifolia* L. *Z. Naturforsch. C* 55, 129–136. doi:10.1515/znc-2000-3-401
- Ahmady-birgani, H., Mirnejad, H., Feiznia, S., and Mcqueen, K. G. (2015). Mineralogy and Geochemistry of Atmospheric Particulates in Western. *Atmos. Environ.* 119, 262–272. doi:10.1016/j.atmosenv.2015.08.021
- Al Omari, M. M. H., Rashid, I. S., Qinna, N. A., Jaber, A. M., and Badwan, A. A. (2016). “Calcium Carbonate,” in *Profiles of Drug Substances, Excipients and Related Methodology*. Editor H. G. Brittain (Amman: Academic Press), 31–132. doi:10.1016/bs.podrm.2015.11.003
- Allen, D. T., Palen, E. J., Haimov, M. I., Hering, S. V., and Young, J. R. (1994). Fourier Transform Infrared Spectroscopy of Aerosol Collected in a Low Pressure Impactor (LPI/FTIR): Method Development and Field Calibration. *Aerosol Sci. Technol.* 21, 325–342. doi:10.1080/02786829408959719
- Andreae, M. O., and Ramanathan, V. (2013). Climate’s Dark Forcings. *Science* 340, 280–281. doi:10.1126/science.1235731
- Atzei, D., Fantauzzi, M., Rossi, A., Fermo, P., Piazzalunga, A., Valli, G., et al. (2014). Surface Chemical Characterization of PM10 Samples by XPS. *Appl. Surf. Sci.* 307, 120–128. doi:10.1016/j.apsusc.2014.03.178
- Atzei, D., and Rossi, A. (2004). Quantitative Surface Analysis of Urban Airborne Particles by X-Ray Photoelectron Spectroscopy. *Ann. Chim.* 94, 123–133. doi:10.1002/adic.200490016
- Bahadur, R., Uplinger, T., Russell, L. M., Sive, B. C., Cliff, S. S., Millet, D. B., et al. (2010). Phenol Groups in Northeastern U.S. Submicrometer Aerosol Particles Produced from Seawater Sources. *Environ. Sci. Technol.* 44, 2542–2548. doi:10.1021/es9032277
- Banerjee, T., Murari, V., Kumar, M., and Raju, M. P. (2015). Source Apportionment of Airborne Particulates through Receptor Modeling: Indian Scenario. *Atmos. Res.* 164–165, 167–187. doi:10.1016/j.atmosres.2015.04.017

AUTHOR CONTRIBUTIONS

Conceptualization, LG; Writing—original draft preparation, LG, AM, FL, and KA; Writing—review and editing, LG, JA, AM, and FL; Characterization, LB-C, DL-S, AR-G, and AC; Data curation, EL, Investigation, JA-B and OK; Supervision, LG.

ACKNOWLEDGMENTS

The authors thank Ing. Armandina Valdez for the use of the monitoring stations of the Sistema Integral de Monitoreo Ambiental (SIMA). The valuable support of Dr. Alonso Concha and M. C. Gerardo Silva Vidaurri from CIMAV.

SUPPLEMENTARY MATERIAL

The Supplementary Material for this article can be found online at: <https://www.frontiersin.org/articles/10.3389/fenvs.2022.929449/full#supplementary-material>

- Barsotti, F., Ghigo, G., and Vione, D. (2016). Computational Assessment of the Fluorescence Emission of Phenol Oligomers: A Possible Insight into the Fluorescence Properties of Humic-like Substances (HULIS). *J. Photochem. Photobiol. A Chem.* 315, 87–93. doi:10.1016/j.jphotochem.2015.09.012
- Birdwell, J. E., and Engel, A. S. (2010). Characterization of Dissolved Organic Matter in Cave and Spring Waters Using UV-Vis Absorbance and Fluorescence Spectroscopy. *Org. Geochem.* 41, 270–280. doi:10.1016/j.orggeochem.2009.11.002
- Bock, S., Kijatkun, C., Berben, D., and Imlau, M. (2019). Absorption and Remission Characterization of Pure, Dielectric (Nano-)powders Using Diffuse Reflectance Spectroscopy: An End-To-End Instruction. *Appl. Sci.* 9, 4933. doi:10.3390/AP9224933
- Bond, T. C., Streets, D. G., Yarber, K. F., Nelson, S. M., Woo, J. H., and Klimont, Z. (2004). A Technology-Based Global Inventory of Black and Organic Carbon Emissions from Combustion. *J. Geophys. Res.* 109, 1–43. doi:10.1029/2003JD003697
- Bradt, R. C. (2008). “The Sillimanite Minerals: Andalusite, Kyanite, and Sillimanite,” in *Ceramic and Glass Materials: Structure, Properties and Processing*. Editors J. F. Shackelford and R. H. Doremus (Boston, MA: Springer US), 41–48. doi:10.1007/978-0-387-73362-3_3
- Bro, R. (1997). PARAFAC. Tutorial and Applications. *Chemom. Intelligent Laboratory Syst.* 38, 149–171. doi:10.1016/S0169-7439(97)00032-4
- Buseck, P. R., and Pósfai, M. (1999). Airborne Minerals and Related Aerosol Particles: Effects on Climate and the Environment. *Proc. Natl. Acad. Sci. U.S.A.* 96, 3372–3379. doi:10.1073/pnas.96.7.3372
- Carmona, J. M., Gupta, P., Lozano-García, D. F., Vanoye, A. Y., Hernández-Paniagua, I. Y., and Mendoza, A. (2021). Evaluation of Modis Aerosol Optical Depth and Surface Data Using an Ensemble Modeling Approach to Assess pm2.5 Temporal and Spatial Distributions. *Remote Sens.* 13, 3102. doi:10.3390/rs13163102
- Chakraborty, A., Ervens, B., Gupta, T., and Tripathi, S. N. (2016). Characterization of Organic Residues of Size-resolved Fog Droplets and Their Atmospheric Implications. *J. Geophys. Res. Atmos.* 121, 4317–4332. doi:10.1002/2015JD024508
- Chen, M., Price, R. M., Yamashita, Y., and Jaffé, R. (2010). Comparative Study of Dissolved Organic Matter from Groundwater and Surface Water in the Florida Coastal Everglades Using Multi-Dimensional Spectrofluorometry Combined

- with Multivariate Statistics. *Appl. Geochem.* 25, 872–880. doi:10.1016/j.apgeochem.2010.03.005
- Chen, P., Kang, S., Li, C., Zhang, Q., Guo, J., Tripathee, L., et al. (2019). Carbonaceous Aerosol Characteristics on the Third Pole: A Primary Study Based on the Atmospheric Pollution and Cryospheric Change (APCC) Network. *Environ. Pollut.* 253, 49–60. doi:10.1016/j.envpol.2019.06.112
- Chen, Q., Chen, Q., Hua, X., Guan, D., and Chang, T. (2021). Gas-phase Brown Carbon: Absorbance and Chromophore Types. *Atmos. Environ.* 264, 118646. doi:10.1016/j.atmosenv.2021.118646
- Chen, Q., Ikemori, F., and Mochida, M. (2016a). Light Absorption and Excitation-Emission Fluorescence of Urban Organic Aerosol Components and Their Relationship to Chemical Structure. *Environ. Sci. Technol.* 50, 10859–10868. doi:10.1021/acs.est.6b02541
- Chen, Q., Miyazaki, Y., Kawamura, K., Matsumoto, K., Coburn, S., Volkamer, R., et al. (2016b). Characterization of Chromophoric Water-Soluble Organic Matter in Urban, Forest, and Marine Aerosols by HR-ToF-AMS Analysis and Excitation-Emission Matrix Spectroscopy. *Environ. Sci. Technol.* 50, 10351–10360. doi:10.1021/acs.est.6b01643
- Chen, Y., Ge, X., Chen, H., Xie, X., Chen, Y., Wang, J., et al. (2018). Seasonal Light Absorption Properties of Water-Soluble Brown Carbon in Atmospheric Fine Particles in Nanjing, China. *Atmos. Environ.* 187, 230–240. doi:10.1016/j.atmosenv.2018.06.002
- Chen, Y., Xie, X., Shi, Z., Li, Y., Gai, X., Wang, J., et al. (2020). Brown Carbon in Atmospheric Fine Particles in Yangzhou, China: Light Absorption Properties and Source Apportionment. *Atmos. Res.* 244, 105028. doi:10.1016/j.atmosres.2020.105028
- Cheng, Y., He, K.-b., Du, Z.-y., Engling, G., Liu, J.-m., Ma, Y.-l., et al. (2016). The Characteristics of Brown Carbon Aerosol during Winter in Beijing. *Atmos. Environ.* 127, 355–364. doi:10.1016/j.atmosenv.2015.12.035
- Chou, C. C.-K., Huang, S.-H., Chen, T.-K., Lin, C.-Y., and Wang, L.-C. (2005). Size-segregated Characterization of Atmospheric Aerosols in Taipei during Asian Outflow Episodes. *Atmos. Res.* 75, 89–109. doi:10.1016/j.atmosres.2004.12.002
- Clean Air Institute (2012). *Air Quality in Latin America: An Overview*. Washington, DC: Clean Air Institute.
- Coury, C., and Dillner, A. M. (2008). A Method to Quantify Organic Functional Groups and Inorganic Compounds in Ambient Aerosols Using Attenuated Total Reflectance FTIR Spectroscopy and Multivariate Chemometric Techniques. *Atmos. Environ.* 42, 5923–5932. doi:10.1016/j.atmosenv.2008.03.026
- Crowley, J. N., Ammann, M., Cox, R. A., Hynes, R. G., Jenkin, M. E., Mellouki, A., et al. (2010). Evaluated Kinetic and Photochemical Data for Atmospheric Chemistry: Volume V - Heterogeneous Reactions on Solid Substrates. *Atmos. Chem. Phys.* 10, 9059–9223. doi:10.5194/acp-10-9059-2010
- D'Andrilli, J., Foreman, C. M., Marshall, A. G., and McKnight, D. M. (2013). Characterization of IHSS Pony Lake Fulvic Acid Dissolved Organic Matter by Electrospray Ionization Fourier Transform Ion Cyclotron Resonance Mass Spectrometry and Fluorescence Spectroscopy. *Org. Geochem.* 65, 19–28. doi:10.1016/j.orggeochem.2013.09.013
- Davarcioglu, B. (2011). Spectral Characterization of Non-clay Minerals Found in the Clays (Central Anatolian-Turkey). *Int. J. Phys. Sci.* 6, 511–522. doi:10.5897/IJPS10.615
- Dittmar, T., and Stubbins, A. (2014). “Dissolved Organic Matter in Aquatic Systems,” in *Treatise on Geochemistry*. Editors H. D. Holland and K. K. Turekian. Second Edition (Oxford: Elsevier), 125–156. doi:10.1016/B978-0-08-095975-7.01010-X
- Dominguez, E., Mercado, J. A., Quesada, M. A., and Heredia, A. (1999). Pollen Sporopollenin: Degradation and Structural Elucidation. *Sex. Plant Reprod.* 12, 171–178. doi:10.1007/s004970050189
- Duan, X., Yan, Y., Li, R., Deng, M., Hu, D., and Peng, L. (2021). Seasonal Variations, Source Apportionment, and Health Risk Assessment of Trace Metals in PM2.5 in the Typical Industrial City of Changzhi, China. *Atmos. Pollut. Res.* 12, 365–374. doi:10.1016/j.apr.2020.09.017
- Duarte, R. M. B. O., Santos, E. B. H., Pio, C. A., and Duarte, A. C. (2007). Comparison of Structural Features of Water-Soluble Organic Matter from Atmospheric Aerosols with Those of Aquatic Humic Substances. *Atmos. Environ.* 41, 8100–8113. doi:10.1016/j.atmosenv.2007.06.034
- Escobedo-Morales, A., Ruiz-López, I. I., Ruiz-Peralta, M. d., Tepech-Carrillo, L., Sánchez-Cantú, M., and Moreno-Orea, J. E. (2019). Automated Method for the Determination of the Band Gap Energy of Pure and Mixed Powder Samples Using Diffuse Reflectance Spectroscopy. *Heliyon* 5, e01505–19. doi:10.1016/j.heliyon.2019.e01505
- Fraund, M., Bonanno, D. J., China, S., Pham, D. Q., Veghte, D., Weis, J., et al. (2020). Optical Properties and Composition of Viscous Organic Particles Found in the Southern Great Plains. *Atmos. Chem. Phys.* 20, 11593–11606. doi:10.5194/acp-20-11593-2020
- Fu, P., Kawamura, K., Chen, J., Qin, M., Ren, L., Sun, Y., et al. (2015). Fluorescent Water-Soluble Organic Aerosols in the High Arctic Atmosphere. *Sci. Rep.* 5, 1–8. doi:10.1038/srep09845
- Gaddam, C. K., and Vander Wal, R. L. (2013). Physical and Chemical Characterization of SIDI Engine Particulates. *Combust. Flame* 160, 2517–2528. doi:10.1016/j.combustflame.2013.05.025
- Gilham, R. J. J., Spencer, S. J., Butterfield, D., Seah, M. P., and Quincey, P. G. (2008). On the Applicability of XPS for Quantitative Total Organic and Elemental Carbon Analysis of Airborne Particulate Matter. *Atmos. Environ.* 42, 3888–3891. doi:10.1016/j.atmosenv.2008.01.007
- Gipson, K., Stevens, K., Brown, P., and Ballato, J. (2015). Infrared Spectroscopic Characterization of Photoluminescent Polymer Nanocomposites. *J. Spectrosc.* 2015, 1–9. doi:10.1155/2015/489162
- González, L. T., Longoria Rodríguez, F. E., Sánchez-Domínguez, M., Cavazos, A., Leyva-Porras, C., Silva-Vidaurri, L. G., et al. (2017). Determination of Trace Metals in TSP and PM 2.5 Materials Collected in the Metropolitan Area of Monterrey, Mexico: A Characterization Study by XPS, ICP-AES and SEM-EDS. *Atmos. Res.* 196, 8–22. doi:10.1016/j.atmosres.2017.05.009
- González, L. T., Longoria-Rodríguez, F. E., Sánchez-Domínguez, M., Leyva-Porras, C., Acuña-Askar, K., Kharissov, B. I., et al. (2018). Seasonal Variation and Chemical Composition of Particulate Matter: A Study by XPS, ICP-AES and Sequential Microanalysis Using Raman with SEM/EDS. *J. Environ. Sci.* 74, 32–49. doi:10.1016/j.jes.2018.02.002
- González, L. T., Rodríguez, F. E. L., Sánchez-Domínguez, M., Leyva-Porras, C., Silva-Vidaurri, L. G., Acuña-Askar, K., et al. (2016). Chemical and Morphological Characterization of TSP and PM2.5 by SEM-EDS, XPS and XRD Collected in the Metropolitan Area of Monterrey, Mexico. *Atmos. Environ.* 143, 249–260. doi:10.1016/j.atmosenv.2016.08.053
- Graber, E. R., and Rudich, Y. (2006). Atmospheric HULIS: How Humic-like Are They? A Comprehensive and Critical Review. *Atmos. Chem. Phys.* 6, 729–753. doi:10.5194/acp-6-729-2006
- Guascito, M. R., Cesari, D., Chirizzi, D., Genga, A., and Contini, D. (2015). XPS Surface Chemical Characterization of Atmospheric Particles of Different Sizes. *Atmos. Environ.* 116, 146–154. doi:10.1016/j.atmosenv.2015.06.028
- Happo, M. S., Salonen, R. O., Hälinen, A. I., Jalava, P. I., Pennanen, A. S., Dormans, J. A. M. A., et al. (2010). Inflammation and Tissue Damage in Mouse Lung by Single and Repeated Dosing of Urban Air Coarse and Fine Particles Collected from Six European Cities. *Inhal. Toxicol.* 22, 402–416. doi:10.3109/08958370903527908
- Hecobian, A., Zhang, X., Zheng, M., Frank, N., Edgerton, E. S., and Weber, R. J. (2010). Water-soluble Organic Aerosol Material and the Light-Absorption Characteristics of Aqueous Extracts Measured over the Southeastern United States. *Atmos. Chem. Phys.* 10, 5965–5977. doi:10.5194/acp-10-5965-2010
- Hoek, G., Mennen, M. G., Allen, G. A., Hofschreuder, P., and Van Der Meulen, T. (1996). Concentrations of Acidic Air Pollutants in The Netherlands. *Atmos. Environ.* 30, 3141–3150. doi:10.1016/1352-2310(96)00032-5
- Huang, R.-J., Yang, L., Cao, J., Chen, Y., Chen, Q., Li, Y., et al. (2018). Brown Carbon Aerosol in Urban Xi'an, Northwest China: The Composition and Light Absorption Properties. *Environ. Sci. Technol.* 52, 6825–6833. doi:10.1021/acs.est.8b02386
- Huertas, J. I., Camacho, D. A., and Huertas, M. E. (2012). Standardized Emissions Inventory Methodology for Open-Pit Mining Areas. *Environ. Sci. Pollut. Res.* 19, 2784–2794. doi:10.1007/s11356-012-0778-3
- Huguet, A., Vacher, L., Relexans, S., Saubusse, S., Froidefond, J. M., and Parlanti, E. (2009). Properties of Fluorescent Dissolved Organic Matter in the Gironde Estuary. *Org. Geochem.* 40, 706–719. doi:10.1016/j.orggeochem.2009.03.002
- Huo, M. Q., Sato, K., Ohizumi, T., Akimoto, H., and Takahashi, K. (2016). Characteristics of Carbonaceous Components in Precipitation and Atmospheric Particle at Japanese Sites. *Atmos. Environ.* 146, 164–173. doi:10.1016/j.atmosenv.2016.07.017

- INECC (2014). Informe nacional de calidad del aire 2013, México. 52.
- Ishii, S. K. L., and Boyer, T. H. (2012). Behavior of Reoccurring PARAFAC Components in Fluorescent Dissolved Organic Matter in Natural and Engineered Systems: A Critical Review. *Environ. Sci. Technol.* 46, 2006–2017. doi:10.1021/es2043504
- Jacobson, M. Z. (2004). Climate Response of Fossil Fuel and Biofuel Soot, Accounting for Soot's Feedback to Snow and Sea Ice Albedo and Emissivity. *J. Geophys. Res.* 109, a–n. doi:10.1029/2004JD004945
- Jacobson, M. Z. (2001). Strong Radiative Heating Due to the Mixing State of Black Carbon in Atmospheric Aerosols. *Nature* 409, 695–697. doi:10.1038/35055518
- Ji, Z., Dai, R., and Zhang, Z. (2015). Characterization of Fine Particulate Matter in Ambient Air by Combining TEM and Multiple Spectroscopic Techniques - NMR, FTIR and Raman Spectroscopy. *Environ. Sci. Process. Impacts* 17, 552–560. doi:10.1039/c4em00678j
- Khare, P., Baruah, B. P., and Rao, P. G. (2011). Water-soluble Organic Compounds (WSOCs) in PM2.5 and PM10 at a Subtropical Site of India. *Tellus, Ser. B Chem. Phys. Meteorol.* 63, 990–1000. doi:10.1111/j.1600-0889.2011.00564.x
- Kim, H., Kim, J. Y., Jin, H. C., Lee, J. Y., and Lee, S. P. (2016). Seasonal Variations in the Light-Absorbing Properties of Water-Soluble and Insoluble Organic Aerosols in Seoul, Korea. *Atmos Environ* 129, 234–242. doi:10.1016/j.atmosenv.2016.01.042
- Kirillova, E. N., Andersson, A., Tiwari, S., Srivastava, A. K., Bisht, D. S., and Gustafsson, Ö. (2014). Water-soluble Organic Carbon Aerosols during a Full New Delhi Winter: Isotope-Based Source Apportionment and Optical Properties. *J. Geophys. Res. Atmos.* 119, 3476–3485. doi:10.1002/2013JD020041
- Kondo, Y., Miyazaki, Y., Takegawa, N., Miyakawa, T., Weber, R. J., Jimenez, J. L., et al. (2007). Oxygenated and Water-Soluble Organic Aerosols in Tokyo. *J. Geophys. Res. Atmos.* 112, D01203. doi:10.1029/2006JD007056
- Lee, H. J., Julie) Laskin, A., Laskin, J., and Nizkorodov, S. A. (2013). Excitation-Emission Spectra and Fluorescence Quantum Yields for Fresh and Aged Biogenic Secondary Organic Aerosols. *Environ. Sci. Technol.* 47, 5763–5770. doi:10.1021/es400644c
- Lee, H. S., Kang, C.-M., Kang, B.-W., and Kim, H.-K. (1999). Seasonal Variations of Acidic Air Pollutants in Seoul, South Korea. *Atmos. Environ.* 33, 3143–3152. doi:10.1016/S1352-2310(98)00382-3
- Leskinen, A., Ruuskanen, A., Kolmonen, P., Zhao, Y., Fang, D., Wang, Q., et al. (2020). The Contribution of Black Carbon and Non-BC Absorbers to the Aerosol Absorption Coefficient in Nanjing, China. *Aerosol Air Qual. Res.* 20, 590–605. doi:10.4209/aaqr.2019.06.0326
- Lin, P., Bluvshstein, N., Rudich, Y., Nizkorodov, S. A., Laskin, J., and Laskin, A. (2017). Molecular Chemistry of Atmospheric Brown Carbon Inferred from a Nationwide Biomass Burning Event. *Environ. Sci. Technol.* 51, 11561–11570. doi:10.1021/acs.est.7b02276
- Liñán-Abanto, R. N., Peralta, O., Salcedo, D., Ruiz-Suárez, L. G., Arnott, P., Paredes-Miranda, G., et al. (2019). Optical Properties of Atmospheric Particles over an Urban Site in Mexico City and a Peri-Urban Site in Queretaro. *J. Atmos. Chem.* 76, 201–228. doi:10.1007/s10874-019-09394-1
- Lippmann, M., Ito, K., Hwang, J.-S., Maciejczyk, P., and Chen, L.-C. (2006). Cardiovascular Effects of Nickel in Ambient Air. *Environ. Health Perspect.* 114, 1662–1669. doi:10.1289/ehp.9150
- Liu, C., Chung, C. E., Yin, Y., and Schnaiter, M. (2018). The Absorption Ångström Exponent of Black Carbon: from Numerical Aspects. *Atmos. Chem. Phys.* 18, 6259–6273. doi:10.5194/acp-18-6259-2018
- Liu, J., Bergin, M., Guo, H., King, L., Kotra, N., Edgerton, E., et al. (2013). Size-resolved Measurements of Brown Carbon in Water and Methanol Extracts and Estimates of Their Contribution to Ambient Fine-Particle Light Absorption. *Atmos. Chem. Phys.* 13, 12389–12404. doi:10.5194/acp-13-12389-2013
- Longoria-Rodríguez, F. E., González, L. T., Mancilla, Y., Acuña-Askar, K., Arizpe-Zapata, J. A., González, J., et al. (2021). Sequential SEM-EDS, PLM, and MRS Microanalysis of Individual Atmospheric Particles: A Useful Tool for Assigning Emission Sources. *Toxics* 9, 37. doi:10.3390/toxics9020037
- Longoria-Rodríguez, F. E., González, L. T., Mendoza, A., Leyva-Porras, C., Arizpe-Zapata, A., Esneider-Alcalá, M., et al. (2020). Environmental Levels, Sources, and Cancer Risk Assessment of PAHs Associated with PM2.5 and TSP in Monterrey Metropolitan Area. *Arch. Environ. Contam. Toxicol.* 78, 377–391. doi:10.1007/s00244-019-00701-1
- López-Ayala, O., González-Hernández, L.-T., Alcantar-Rosales, V.-M., Elizarragaz-de la Rosa, D., Heras-Ramírez, M.-E., Silva-Vidaurre, L.-G., et al. (2019). Levels of Polycyclic Aromatic Hydrocarbons Associated with Particulate Matter in a Highly Urbanized and Industrialized Region in Northeastern Mexico. *Atmos. Pollut. Res.* 10, 1655–1662. doi:10.1016/j.apr.2019.06.006
- Lu, S., Hao, X., Liu, D., Wang, Q., Zhang, W., Liu, P., et al. (2016). Mineralogical Characterization of Ambient Fine/ultrafine Particles Emitted from Xuanwei C1 Coal Combustion. *Atmos. Res.* 169, 17–23. doi:10.1016/j.atmosres.2015.09.020
- Makula, P., Pacia, M., and Macyk, W. (2018). How to Correctly Determine the Band Gap Energy of Modified Semiconductor Photocatalysts Based on UV-Vis Spectra. *J. Phys. Chem. Lett.* 9, 6814–6817. doi:10.1021/acs.jpcclett.8b02892
- Mancilla, Y., Herckes, P., Fraser, M. P., and Mendoza, A. (2015). Secondary Organic Aerosol Contributions to PM2.5 in Monterrey, Mexico: Temporal and Seasonal Variation. *Atmos. Res.* 153, 348–359. doi:10.1016/j.atmosres.2014.09.009
- Mancilla, Y., Hernandez Paniagua, I. Y., and Mendoza, A. (2019). Spatial Differences in Ambient Coarse and Fine Particles in the Monterrey Metropolitan Area, Mexico: Implications for Source Contribution. *J. Air & Waste Manag. Assoc.* 69, 548–564. doi:10.1080/10962247.2018.1549121
- Mancilla, Y., Mendoza, A., Fraser, M. P., and Herckes, P. (2016). Organic Composition and Source Apportionment of Fine Aerosol at Monterrey, Mexico, Based on Organic Markers. *Atmos. Chem. Phys.* 16, 953–970. doi:10.5194/acp-16-953-2016
- Maria, S. F., Russell, L. M., Turpin, B. J., and Porcja, R. J. (2002). FTIR Measurements of Functional Groups and Organic Mass in Aerosol Samples over the Caribbean. *Atmos. Environ.* 36, 5185–5196. doi:10.1016/S1352-2310(02)00654-4
- Martin, S. T., Hung, H.-M., Park, R. J., Jacob, D. J., Spurr, R. J. D., Chance, K. V., et al. (2004). Effects of the Physical State of Tropospheric Ammonium-Sulfate-Nitrate Particles on Global Aerosol Direct Radiative Forcing. *Atmos. Chem. Phys.* 4, 183–214. doi:10.5194/acp-4-183-2004
- Martinez, M. A., Caballero, P., Carrillo, O., Mendoza, A., and Mejia, G. M. (2012). Chemical Characterization and Factor Analysis of PM2.5 in Two Sites of Monterrey, Mexico. *J. Air & Waste Manag. Assoc.* 62, 817–827. doi:10.1080/10962247.2012.681421
- Matos, J. T. V., Freire, S. M. S. C., Duarte, R. M. B. O., and Duarte, A. C. (2015). Natural Organic Matter in Urban Aerosols: Comparison between Water and Alkaline Soluble Components Using Excitation-Emission Matrix Fluorescence Spectroscopy and Multiway Data Analysis. *Atmos. Environ.* 102, 1–10. doi:10.1016/j.atmosenv.2014.11.042
- McKnight, D. M., Boyer, E. W., Westerhoff, P. K., Doran, P. T., Kulbe, T., and Andersen, D. T. (2001). Spectrofluorometric Characterization of Dissolved Organic Matter for Indication of Precursor Organic Material and Aromaticity. *Limnol. Oceanogr.* 46, 38–48. doi:10.4319/lo.2001.46.1.0038
- Menges, F. (2020). "Spectragryph-Optical Spectroscopy Software," Version 1.2.15, 2020. Available at: <http://www.ffmpeg2.de/spectragryph/>.
- Miyazaki, Y., Kondo, Y., Shiraiwa, M., Takegawa, N., Miyakawa, T., Han, S., et al. (2009). Chemical Characterization of Water-Soluble Organic Carbon Aerosols at a Rural Site in the Pearl River Delta, China, in the Summer of 2006. *J. Geophys. Res.* 114. doi:10.1029/2009JD011736
- Mladenov, N., Alados-Arboledas, L., Olmo, F. J., Lyamani, H., Delgado, A., Molina, A., et al. (2011). Applications of Optical Spectroscopy and Stable Isotope Analyses to Organic Aerosol Source Discrimination in an Urban Area. *Atmos. Environ.* 45, 1960–1969. doi:10.1016/j.atmosenv.2011.01.029
- Mo, Y., Li, J., Cheng, Z., Zhong, G., Zhu, S., Tian, C., et al. (2021). Dual Carbon Isotope-Based Source Apportionment and Light Absorption Properties of Water-Soluble Organic Carbon in PM2.5 over China. *JGR Atmos.* 126, 1–13. doi:10.1029/2020JD033920
- Moosmüller, H., Chakrabarty, R. K., Ehlers, K. M., and Arnott, W. P. (2011). Absorption Ångström Coefficient, Brown Carbon, and Aerosols: Basic Concepts, Bulk Matter, and Spherical Particles. *Atmos. Chem. Phys.* 11, 1217–1225. doi:10.5194/acp-11-1217-2011
- Morozzi, P., Ballarin, B., Arcozzi, S., Brattich, E., Lucarelli, F., Nava, S., et al. (2021). Ultraviolet-Visible Diffuse Reflectance Spectroscopy (UV-Vis DRS), a Rapid and Non-destructive Analytical Tool for the Identification of Saharan Dust Events in Particulate Matter Filters. *Atmos. Environ.* 252, 118297. doi:10.1016/j.atmosenv.2021.118297
- Murphy, K. R., Hambly, A., Singh, S., Henderson, R. K., Baker, A., Stuetz, R., et al. (2011). Organic Matter Fluorescence in Municipal Water Recycling

- of Asian Dust: Optical Properties, Chemical Compositions, and Potential Sources. *Sci. Total Environ.* 789, 147971. doi:10.1016/j.scitotenv.2021.147971
- Wonaschütz, A., Hitzengerger, R., Bauer, H., Pouresmaeil, P., Klatzer, B., Caseiro, A., et al. (2009). Application of the Integrating Sphere Method to Separate the Contributions of Brown and Black Carbon in Atmospheric Aerosols. *Environ. Sci. Technol.* 43, 1141–1146. doi:10.1021/es8008503
- Wu, C., Wang, G., Li, J., Li, J., Cao, C., Ge, S., et al. (2020). The Characteristics of Atmospheric Brown Carbon in Xi'an, Inland China: Sources, Size Distributions and Optical Properties. *Atmos. Chem. Phys.* 20, 2017–2030. doi:10.5194/acp-20-2017-2020
- Wu, G., Fu, P., Ram, K., Song, J., Chen, Q., Kawamura, K., et al. (2021). Fluorescence Characteristics of Water-Soluble Organic Carbon in Atmospheric Aerosol[☆]. *Environ. Pollut.* 268, 115906. doi:10.1016/j.envpol.2020.115906
- Wu, G., Ram, K., Fu, P., Wang, W., Zhang, Y., Liu, X., et al. (2019). Water-Soluble Brown Carbon in Atmospheric Aerosols from Godavari (Nepal), a Regional Representative of South Asia. *Environ. Sci. Technol.* 53, 3471–3479. doi:10.1021/acs.est.9b00596
- Wünsch, U. J., and Murphy, K. (2021). A Simple Method to Isolate Fluorescence Spectra from Small Dissolved Organic Matter Datasets. *Water Res.* 190, 116730. doi:10.1016/j.watres.2020.116730
- Xu, P., Xu, J., He, M., Song, L., Chen, D., Guo, G., et al. (2016). Morphology and Chemical Characteristics of Micro- and Nano-Particles in the Haze in Beijing Studied by XPS and TEM/EDX. *Sci. Total Environ.* 565, 827–832. doi:10.1016/j.scitotenv.2016.03.042
- Yan, C., Zheng, M., Sullivan, A. P., Bosch, C., Desyaterik, Y., Andersson, A., et al. (2015). Chemical Characteristics and Light-Absorbing Property of Water-Soluble Organic Carbon in Beijing: Biomass Burning Contributions. *Atmos. Environ.* 121, 4–12. doi:10.1016/j.atmosenv.2015.05.005
- Yan, G., and Kim, G. (2017). Speciation and Sources of Brown Carbon in Precipitation at Seoul, Korea: Insights from Excitation-Emission Matrix Spectroscopy and Carbon Isotopic Analysis. *Environ. Sci. Technol.* 51, 11580–11587. doi:10.1021/acs.est.7b02892
- Yan, J., Wang, X., Gong, P., Wang, C., and Cong, Z. (2018). Review of Brown Carbon Aerosols: Recent Progress and Perspectives. *Sci. Total Environ.* 634, 1475–1485. doi:10.1016/j.scitotenv.2018.04.083
- Yang, Y., Qin, J., Qi, T., Zhou, X., Chen, R., Tan, J., et al. (2020). Fluorescence Characteristics of Particulate Water-Soluble Organic Compounds Emitted from Coal-Fired Boilers. *Atmos. Environ.* 223, 117297. doi:10.1016/j.atmosenv.2020.117297
- Yu, X., Song, W., Yu, Q., Li, S., Zhu, M., Zhang, Y., et al. (2018). Fast Screening Compositions of PM2.5 by ATR-FTIR: Comparison with Results from IC and OC/EC Analyzers. *J. Environ. Sci.* 71, 76–88. doi:10.1016/j.jes.2017.11.021
- Yuan, W., Huang, R.-J., Yang, L., Guo, J., Chen, Z., Duan, J., et al. (2020). Characterization of the Light-Absorbing Properties, Chromophore Composition and Sources of Brown Carbon Aerosol in Xi'an, Northwestern China. *Atmos. Chem. Phys.* 20, 5129–5144. doi:10.5194/acp-20-5129-2020
- Yue, Y., Cheng, J., Lee, K. S., Stocker, R., He, X., Yao, M., et al. (2022). Effects of Relative Humidity on Heterogeneous Reaction of SO₂ with CaCO₃ Particles and Formation of CaSO₄·2H₂O Crystal as Secondary Aerosol. *Atmos. Environ.* 268, 118776. doi:10.1016/j.atmosenv.2021.118776
- Zarasvandi, A., Carranza, E. J. M., Moore, F., and Rastmanesh, F. (2011). Spatio-Temporal Occurrences and Mineralogical-Geochemical Characteristics of Airborne Dusts in Khuzestan Province (Southwestern Iran). *J. Geochemical. Explor.* 111, 138–151. doi:10.1016/j.gexplo.2011.04.004
- Zapata-Hernandez, C., Durango-Giraldo, G., Tobón, C., and Buitrago-Sierra, R. (2020). Physicochemical Characterization of Airborne Particulate Matter in Medellín, Colombia, and its Use in an In Silico Study of Ventricular Action Potential. *Water. Air. Soil Pollut.* 231, 508. doi:10.1007/s11270-020-04884-5
- Zeb, B., Alam, K., Sorooshian, A., Blaschke, T., Ahmad, I., and Shahid, I. (2018). On the Morphology and Composition of Particulate Matter in an Urban Environment. *Aerosol Air Qual. Res.* 18, 1431–1447. doi:10.4209/aaqr.2017.09.0340
- Zent, A. P., Ichimura, A. S., Quinn, R. C., and Harding, H. K. (2008). The Formation and Stability of the Superoxide Radical (O₂⁻) on Rock-Forming Minerals: Band Gaps, Hydroxylation State, and Implications for Mars Oxidant Chemistry. *J. Geophys. Res.* 113, 1–13. doi:10.1029/2007JE003001
- Zhan, Y., Tsou, N. T., Li, J., Chen, Q., and Du, L. (2022). Water-soluble Matter in PM2.5 in a Coastal City over China: Chemical Components, Optical Properties, and Source Analysis. *J. Environ. Sci.* 114, 21–36. doi:10.1016/j.jes.2021.07.011
- Zhou, Y., Xiao, H., Guan, H., Zheng, N., Zhang, Z., Tian, J., et al. (2020). Chemical Composition and Seasonal Variations of PM2.5 in an Urban Environment in Kunming, SW China: Importance of Prevailing Westerlies in Cold Season. *Atmos. Environ.* 237, 117704. doi:10.1016/j.atmosenv.2020.117704
- Zhuo, J. F., Guo, W. D., Deng, X., Zhang, Z. Y., Xu, J., and Huang, L. F. (2010). [Fluorescence Excitation-Emission Matrix Spectroscopy of CDOM from Yundang Lagoon and its Indication for Organic Pollution]. *Guang Pu Xue Yu Guang Pu Fen Xi* 30, 1539–1544.
- Zwinkels, J., Germer, T., and Tsai, B. (2014). *Experimental Methods in the Physical Sciences Spectrophotometry: Accurate Measurement of Optical Properties of Materials*, 1–10. Amsterdam, Netherlands: Elsevier.

Conflict of Interest: The authors declare that the research was conducted in the absence of any commercial or financial relationships that could be construed as a potential conflict of interest.

Publisher's Note: All claims expressed in this article are solely those of the authors and do not necessarily represent those of their affiliated organizations, or those of the publisher, the editors and the reviewers. Any product that may be evaluated in this article, or claim that may be made by its manufacturer, is not guaranteed or endorsed by the publisher.

Copyright © 2022 Acuña Askar, González, Mendoza, Kharissova, Rodríguez-Garza, Lara, Campos, López-Serna, Bautista-Carrillo, Alfaro-Barbosa and Longoria-Rodríguez. This is an open-access article distributed under the terms of the Creative Commons Attribution License (CC BY). The use, distribution or reproduction in other forums is permitted, provided the original author(s) and the copyright owner(s) are credited and that the original publication in this journal is cited, in accordance with accepted academic practice. No use, distribution or reproduction is permitted which does not comply with these terms.